# 博士 論 文

題　　目

**Pore size distribution control of potassium and metakaolin based geopolymers**

**(メタカオリンとカリウムを基質とするジオポリマーの細孔径分布制御)**


指　導　教　員
末松 久幸　教　授

著　者

18507884　　楊婭茹


令和 5 年 6 月 26 日


長岡技術科学大学大学院博士後期課程

エネルギー・環境工学専攻

# Abstract

Geopolymers are generally three-dimensional networks formed by aluminosilicate tetrahedral structures bonded by covalent bonds of oxygen atoms. Due to its special porous structure, geopolymer itself has many excellent physical and chemical properties, for example it has high porosity, heat resistance and good mechanical strength as well as chemical inertness compared to conventional cements. Therefore, geopolymers are often used as alternatives to concrete for insulation and radioactive waste solidification. In this study geopolymers were attempted to apply catalyst support in PAR and for radioactive aluminum compaction in JMTR by controlling the pore size distribution of potassium-based metakaolin geopolymers.

The geopolymers in this study were made from metakaolin powder, AFACO silica, potassium silicate solutions ($K_2SiO_3$) and potassium hydroxide (KOH). The ratio of Al: Si: K: $H_2O$ is 1:2.1:0.8:8. This ratio was used to synthesized geopolymer, the different post curing conditions after 4 days initial cured at 60℃ was conducted. The result showed that the average pore size of the demolded (quick dehydration) and uncapped (slow dehydration) samples was almost the same. This means that porosity may form at a certain viscosity in the first 4 days. A single chemical reaction (dehydration) was likely to be the origin of the pore formation and to take place at the same viscosity and irrelevant to the curing condition.

In the next research geopolymer samples were synthesized with the same molar ratios and cured sample at 60℃ from 1 to 4 days but different post curing conditions (open lid and with lid) for studying the air tightness on pore forming process. The results showed that the pores were with similar average sizes and might have been formed within a day. The average pore sizes of the samples without lid were larger than or the same as the one covered with lid. In the sample with lid, the water was kept in the mold, it might increase the pressure inside the mold, the pressure on the internal pores increased and the formation of larger pores was hindered. This may result in the formation of smaller pores in the samples with lid.

In this thesis geopolymers were used to compact radioactive aluminum material. The geopolymers synthesized here have various water content and cure at different initial temperatures. After electron irradiation up to 992 kGy, the Vickers hardness at 110 MPa did not change significantly

with water content. The geopolymers in this study are stable enough to be used as catalyst support materials and compaction materials for radioactive aluminum ions.

# Acknowledgments

This paper has received a lot of effort and support. I would like to express my thanks to everyone who helped me with my thesis.

First, I would like to thank my supervisor, Prof. Hisayuki Suematsu. He patiently guided my studies and supported me in my life during my graduate and Ph.D. He provided me with a lot of good advice, and every time I had a problem with my research, he always gave me a lot of directions to think about, which made me suddenly enlightened and encouraged. With his support, I was able to live a very full and active life during my PhD.

Second, I would like to especially thank my co-advisors Prof. Thorogood, Prof. Tatsuya Suzuki, Prof. Niihara, Prof. Nakayama for their valuable help and advice during my Ph.D. Without their invaluable guidance and support, this thesis would not have been possible. Next, I would like to thank Tohoku University for providing experimental instruments. And the enthusiastic help from the staff and Fauzia Hanum Ikhwan during our experiment.

I would like to thank all the students in Suematsu's laboratory for their kind help when I needed support on the experiments. I would also like to especially thank Ms. Le Thi Chau Duyen, she is not only my friend, but also helped me and gave me a lot of support and advice when I encountered problems and doubts in my research. Then I would like to thank Xianglin Meng for joining me in my final year of PhD. and added a lot of fun to my life.

Finally, I would like to thank my parents for their financial and emotional support and their encouragement and patience throughout my long academic journey.

# List of tables

# List of figures

# Table of Contents

# 1. Introduction

## 1.1 Background

As we all know, ordinary portland cement (OPC) has always been an indispensable industrial material in our life. Many papers have suggested the significant contribution of OPC to $CO_2$ emissions [1,2]. Judging whether an industrial material is good or bad is not only an environmental issue, but also whether its durability and raw materials are easy to obtain and cost-effective. Due to the lower fineness of OPC, hence has higher permeability and as a result it has lower durability [3]. Therefore, it is a new challenge to search for alternative types of cementitious materials.

Geopolymers can be synthesized at room temperature and are therefore more cost-effective than synthesizing aluminosilicate compounds and zeolite structures simultaneously at a high temperature. Geopolymer binders are superior to OPC in terms of synthesis conditions, mechanical properties, the cost of raw material and durability.

Geopolymer was named by Prof. J. Davidovits in 1978 and described as a green cementitious material without cement. Geopolymers are inorganic polymers obtained by alkaline activation of aluminosilicate materials such as fly ash. Their properties are like natural rocks in structure and chemical. Geopolymers are named geopolymers because they are synthesized by condensation mechanisms, such as thermosetting organic polymers. Geopolymers can be defined as covalently bonded amorphous Si-O-Al networks. Among them, the $SiO_4$ and $AlO_4$ tetrahedral frameworks are connected by sharing oxygen atoms, and the dehydration to form a dense amorphous to semi-crystalline three-dimensional network structure. These are called geopolymers because their starting materials are derived from geological sources and the formation of geopolymers is carried out by inorganic polymerization and condensation reactions [4].

## 1.2. Purpose and objectives

Due to its special porous structure, geopolymer itself has many excellent physical and chemical properties, such as high porosity, high temperature resistance, chemical stability. Therefore, geopolymers are often used as structure material, alternative material for concrete, porous insulation materials, and for solidification of radioactive waste.

In order to further adapt the geopolymer to specific applications. For example, some

applications may require increased porosity (such as catalyst support in PAR) and some applications may require decreased porosity (such as compact radioactive ions). If the porosity of geopolymers can be well controlled, it will make better use of this clean and environmentally friendly material.

- Therefore, this thesis will study to control the pore distribution of potassium-based kaolin geopolymers.

The purpose and objectives of this thesis include but are not limited to the following:

- Effects of initial curing temperature and later curing conditions on the stability, pore size distribution and mechanical properties of geopolymers
- Whether the pore size distribution is affected by the curing condition, here specifically refers to the closed lid or open lid during the curing process.
- Pore size distribution of potassium and metakaolin based geopolymers with different water contents under electron radiation.

## 1.2 Thesis outline

To address all our goals and questions, we need to develop a coherent research plan. This thesis includes 7 chapters in total.

Chapter 1 gives a preliminary introduction to geopolymer concrete.

Chapter 2 a summary of the literature of studies related to geopolymers is provided.

Chapter 3 describes the materials and testing procedures used in this paper.

Chapter 4 explores the pore distribution of geopolymers under different dehydration conditions. The degree of shrinkage and the surface of the sample were used to know the effect of the temperature on the mechanical properties of potassium and metakaolin based geopolymer. scanning electron microscope (SEM) was used to analyze the pore size distribution of the samples. As well as X-ray diffraction (XRD) and thermogravimetry-differential thermal analysis (TG-DTA) to analyze the curing conditions of the samples for high temperature tolerance of potassium and metakaolin based geopolymers.

Chapter 5 further explores the pore size distribution based on Chapter 4. In the case of ensuring the same curing temperature, the isolation of air is used as a variable in the curing process. The experiment mainly focuses on the pore distribution, Vickers hardness and XRD.

Chapter 6 combines the practical application and the previous study in this thesis of pores to

conduct electron radiation experiments on geopolymers. As we all know, a series of problems may be caused by the radiolysis of water. With this background. The influence of water on pores size distribution and hardness is considered. The water content of the samples when they were synthesized and conducted experiments on their hardness before and after electron irradiation, further confirming the possibility of our samples in the practical application of nuclear waste treatment.

Chapter 7 makes a detailed summary of this thesis.

Chapter 8 proposes a possible future research plan.

# 2. Literature review

## 2.1 An overview of geopolymers

Geopolymerization is a process in which inorganic materials, such as kaolin, zeolite, fly ash, or clay, are chemically transformed into a solid material with properties like traditional cement-based materials. It involves the reaction of source materials with alkaline activators to produce a geopolymer binder.

The key ingredients involved in geopolymerization are source materials and alkaline activators. Industrial by-products such as clay, fly ash from coal combustion, or slag from metal smelting processes, naturally occurring materials such as kaolin can all be source materials. Alkaline activators are usually solutions containing alkali metal hydroxides or silicates, such as sodium hydroxide or sodium silicate.

The geopolymerization process begins by dissolving the source material in a solution of alkaline activator, which forms a liquid phase. This liquid phase undergoes a complex series of chemical reactions, including polymerization and condensation, to form a three-dimensional skeleton structure of geopolymer chains. The process of geological aggregation has been mentioned in many literatures [5.6]. Figure 1 is the process of geological aggregation [7, 8,9].

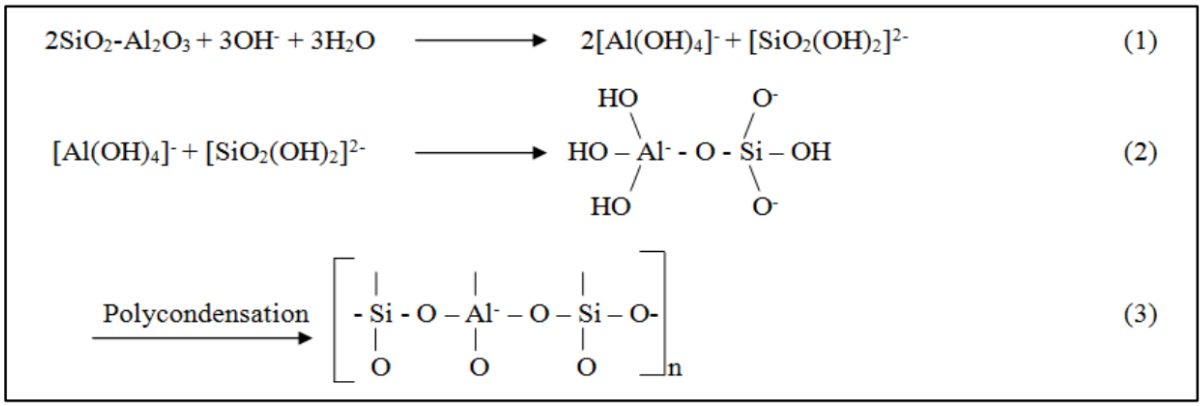


**Fig.1.** Three steps of geopolymerization process [7].

Silicon (Si), aluminum (Al) and oxygen (O) are the main constituent elements of geopolymers. Silicon and oxygen in the silicate feedstock play key roles in the polymer formation process. They form silicon-oxygen bonds through polymerization and solidification reactions, forming a three-dimensional network structure. Aluminum mainly exists in raw materials and can form aluminum-silicon-oxygen bonds together with silicon during the polymerization process, further enhancing

the structural stability of the polymer. The elemental ratio of a geopolymer largely determines its microstructure [10,11,12]. Figure 2 shows the different types of structures produced by different Si-Al ratios [13].

## 2.2 Raw materials

Geopolymers can be synthesized from many different raw materials, including natural materials as well as industrial by-products. The choice of raw material depends on various factors such as cheap and easy availability. Environmental protection, reactivity, desired properties of geopolymers and specific application requirements. Utilizing these raw materials in geopolymerization has the advantage of recycling industrial by-products and mitigating the environmental impact of industrial waste. For example, fly ash is the powdery residue produced after the combustion of pulverized coal in coal-fired power plants. Its composition contains high silica (Si) and alumina (Al) contents, making it a widely used raw material for the production of geopolymers [14,15,15,17,18].

Slag is a by-product of metal smelting processes such as iron and steel smelting. It is rich in silica and alumina, so it can be used as a raw material for synthetic geopolymers [19,20].

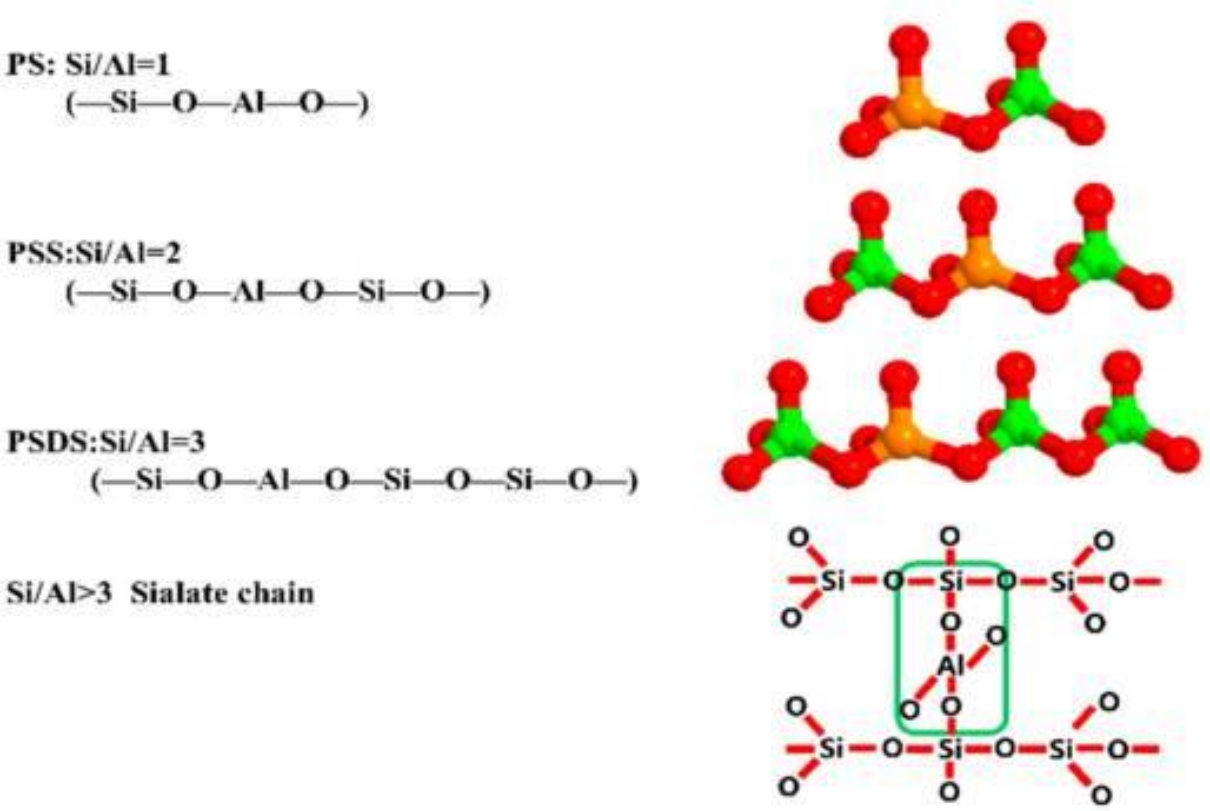


**Fig. 2** shows the different types of structures produced by different Si-Al ratios [13].

Metakaolin: Metakaolin is heat-treated kaolin. It is commonly used to produce geopolymer due to its high reactivity and purity. Metakaolin is rich in alumina and silica, which help to form a strong geopolymer matrix. [21,22,23].

Rice husk ash: Rice husk, a by-product of rice milling, is burned to produce rice husk ash. Because it contains a large amount of amorphous silica, it can be used as a raw material for synthetic geopolymers. [24,25,26].

Natural clays: Naturally occurring clays, such as kaolin and bentonite. Those are used as raw materials to synthesize geopolymer. These clays contain silica and alumina, which are essential for geopolymerization. [27,28].

Silicon powder: It is a by-product of the production process of silicon and ferrosilicon alloy. It is rich in silica and therefore highly reactive and is often used as an auxiliary material in the production of geopolymers. [29,30].

## 2.3 Alkaline activator

Alkali activators in geopolymers play an important role in initiating and promoting geopolymerization. It acts as a catalyst by providing the necessary alkalinity and soluble alkali ions, which are essential for the dissolution, polymerization, and condensation reactions of source materials.

Alkali activators are usually dissolved in water as hydroxides or silicates to release hydroxide (OH-) ions or alkali metal cations such as sodium or potassium. These alkaline substances have a high pH, creating the alkaline environment required for geopolymerization. The alkaline environment provided by the alkaline activator can promote the dissolution of the raw material, and the dissolution process releases reactive silica and alumina species from the raw material, followed by a series of polymerization and condensation reactions under the action of the alkaline activator [31, 32]

The alkalinity of the activator helps to promote the formation of a three-dimensional network structure of the geopolymer skeleton. Alkali ions from activator can replace the cations present in the source material, forming strong and stable geopolymer bonds. The alkalinity and soluble alkali ions provided by the activator help to form a dense and dense geopolymer matrix, which improves mechanical properties such as compressive strength [33]

The concentration and type of base activators affect the geopolymerization kinetics and thus the cure time, processability and final physicochemical properties of the geopolymer. By adjusting

the activator composition, the rate of geopolymerization can be controlled to meet specific application requirements.

There are many common base activators such as sodium hydroxide (NaOH) [34,35], potassium hydroxide (KOH) [36,37], potassium silicate ($K_2SiO_3$) [38,39], and sodium silicate ($Na_2SiO_3$) [40,41].

## 2.4 Geopolymer characterization

Evaluation of the performance, durability, and suitability of geopolymers for specific applications is required.

For example, compressive strength is an important parameter for the mechanical properties of geopolymers. Cured geopolymer samples were measured by subjecting them to compressive forces using standardized testing procedures. [42,43].

The ability of geopolymers to resist bending or deformation is usually measured using flexural strength. It is determined by subjecting the sample to bending forces using the appropriate test method [44,45].

Microstructural analysis involves examining geopolymer materials at the microscopic level. Using techniques such as SEM and transmission electron microscopy (TEM) can yield information about the internal structure of geopolymers and the distribution of phases and components, including the morphology of geopolymer material and the existence or absence of any pores or fractures. [46,47].

Analyzing the mineral composition of geopolymer samples and identifying the presence of crystalline phases typically uses X-ray diffraction, by which the amorphous content is measured to determine the degree of geopolymerization. [48,49].

Fourier transform infrared (FTIR) spectroscopy is applied to analyze the chemical bonds and functional groups that exist in geopolymer matrices. It can provide information on the formation and degree of polymerization of geopolymer bonds [50,51,52].

Thermal analysis techniques, like thermogravimetric analysis (TGA) and differential scanning calorimetry (DSC), can be applied to evaluate heat stability, decomposition behavior and phase transition of geopolymers at different temperatures. [53,54].

The porosity and permeability of geopolymer samples determine their resistance to fluid flow and can affect their durability and resistance to chemical attack. Techniques such as mercury porosimetry and permeability testing can be used to quantify these properties. [55,56,57].

# 3. Experimental procedure

## 3.1 Materials

In this thesis the source material for geopolymer were provided by a Japanese company called AVAN ENG co. ltd.

**Potassium hydroxide:**

Potassium hydroxide, generally known as caustic potash, is a potent base and is an inorganic compound. Its chemical formula is KOH. There are many forms of sales in the market, including granules, flakes, and powder. In this thesis, pellets are used for the synthesis of geopolymers. Potassium hydroxide is also a precursor to other potassium-based compounds, which can be applied in various chemical, industrial, and manufacturing applications. Potassium hydroxide can be used as a stabilizer and thickener and can be used to adjust pH in food.

Apart from the uses mentioned above, KOH is applied in soap making, conducting electrolytes in alkaline batteries, electroplating, photolithography, paint, and varnish removers, among many other applications.

For this research the potassium hydroxide was manufactured by UNID.CO.LTD. The freezing point / melting point was 380 degrees, and the specific gravity was 2.044. CAS. No is 1310-58-3.

**Potassium silicate solution:**

The properties of potassium silicate vary with the ratio of silica to potassium oxide. The proportions were changed to meet the requirements of extensive customization. The product is usually available in the market as an aqueous solution or as a solid in glassy flakes (Wako concentration, 50%) and this solution was used in this paper.

Potassium silicate glass is a colorless supercooled melt of potassium carbonate and pure silica sand. Potassium silicate, although slightly hygroscopic, will remain unrestricted flow if kept in airtight drums. Potassium silicate solutions are produced by dissolving potassium silicate glass in hot water. It is possible to produce clearly defined but very different products by changing the ratio of silica to potassium oxide.

Viscosity is a function of the silica-to-potassium oxide ratio, and the solid contents: as either of these variables decreases, the viscosity is reduced. Viscosity is also a function of the water content of the solution and the temperature of the solution (Relatively small changes in water content have

a significant effect on viscosity). The pH of potassium silicate is a function of composition and concentration. A good method to consider potassium silicate solution is as a polymer solution of SiOx-SiOx oligomers, Stabilized by $K_2O$ (another expression of KOH: $H_2O$). By changing the pH, for instance, eliminating or neutralizing an excess of the KOH will lead to faster develop the large chains of SiOx. This may increase viscosity and can go so far as to lead to complete gelation of the silica portion.

**EFACO silica:**

Silicon dioxide, the chemical formula is $SiO_2$. It is an acidic oxide, and its hydrate is silicic acid ($H_2SiO_3$). As is well-known silica is most found in nature, quartz, and various kinds of living organisms. Silica is the main component of sand in many places of the world. Silica is one of the most complicated and luxuriant materials. It is both polylineal and synthetically produced. As we all know, fused silica, silica gel, crystal, fumed silica, and aerogels.

$SiO_2$ crystals have various crystal forms, and the basic structural unit is a tetrahedron. Each Si is combined with 4 O, Si is at the center, and O is at four vertices; there are 6 silicon atoms and six oxygen atoms on the smallest ring. Many such tetrahedrons are connected by O at the vertex, each O is shared by two tetrahedrons, that is, each O is combined with 2 Si. In fact, $SiO_2$ crystal is a crystal with a three-dimensional network structure composed of Si and O in a ratio of 1:2. Therefore, $SiO_2$ is generally used to represent the composition of silica. $SiO_4$ tetrahedron exists not only in $SiO_2$ crystals, but also in all silicate ores, and it is the basic skeleton of the colorful silicate world.

In this research, EFACO silica was used to synthesis geopolymer, the details information is shown in Table. 1.

Table. 1. The details of EFACO silica in this experiment [58]

| Elkem Microsilica 951 Chemical Analysis(weight%) | | |
|---|---|---|
| Product name | | EFACO |
| Origin | | Egypt |
| Analysis items | | Specification |
| $SiO_2$ | % min. | 94.0 |
| C | % max. | 2.0 |
| $Fe_2O_3$ | % max. | 1.0 |
| $Al_2O_3$ | % max. | 1.0 |
| CaO | % max. | 1.0 |
| MgO | % max. | 1.0 |
| $K_2O$ | % max. | 1.2 |
| $Na_2O$ | % max. | 0.5 |
| $H_2O$ | % max. | 1.0 |

**Metakaolin:**

The quality and reactivity of metakaolin depends to a large extent on the properties of the raw materials applied. Metakaolin can be yielded from all kinds of natural sources including kaolinite: High purity kaolinite deposits, low purity kaolinite deposits or tropical soils, paper sludge wastes, oil sand tailings, and metakaolinite.

In this research, metakaolin was purchased from Imerys-specialities in Japan under the brand name PoleStar450. Determination of chemical composition of metakaolin by X-ray fluorescence method was $Al_2O_3 \cdot 2{\sim}3SiO_2$ powders (the details is shown in Table .2.) and were used. For a foaming agent, Distilled water was added.

Table. 2. The details of metakaolin in this experiment [59].

| Chemical Analysis of metakaolin by XRF (weight%) | |
|---|---|
| Product name | Metakaolin |
| Origin | China |
| Analysis items | Specification |
| $SiO_2$ | 51.19 |
| $Al_2O_3$ | 45.71 |
| $Fe_2O_3$ | 0.54 |
| $TiO_2$ | 1.10 |
| CaO | 0.2 |
| MgO | 0.08 |
| $K_2O$ | 0.14 |
| $Na_2O$ | 0.18 |
| LOI | 0.73 |
| $P_2O_5$ | 0.12 |

## 3.2 Research Methodology

### 3.2.1 Cutting machine

**Fig.3** The cutting machine

To measure the pore size distribution of internal cross-sections of geopolymers, the sample should be cut out for subsequent detection of the pore size using a scanning electron microscope.

Figure 3 shows the cutting machine used in this thesis. Samples were cut 5mm from the bottom. The cutting process needs to be uniform and slow to prevent sample breakage or uneven cutting surface caused by unstable cutting process. The cutting process of each sample takes about 40 minutes to complete.

### 3.2.2 SEM

TM3000 Miniscope, HITACHI, is shown in Fig. 4. This device is designed to be energy efficient and does not require a continuous power supply. It can boot in about three minutes. Low-vacuum type and immediate response to any large magnification, this device supports magnifications from 15x to 30,000x. Three observation conditions can be set: surface observation, normal observation, and high-intensity observation, and it has automatic functions such as automatic start, automatic focus, and automatic brightness. Equipped with image shift function and high operability of operation buttons, it enables deep-focus 3D morphology observation.


**Fig.4** Scanning Electron Microscope-SEM

In this paper this device was used to take 50 images from cross-sections, measure and count the pore sizes, and classify them by size to know pore size distribution map of the sample.

### 3.2.3 XRD

XRD is one of the most crucial non-destructive research instruments used for analyzing everything from liquids to powders and crystals. From research to production, XRD is an indispensable method for material microscopic characterization and quality detection. The crystal phases of various materials are identified by XRD technology, and quantitative analysis of the phases is carried out after identification. X-ray diffraction is excellent at clarifying the three-dimensional atomic structure of crystalline solids. The properties and functions of materials depend largely on the microstructure of crystals. Therefore, XRD technology has been widely used in material research, development, and production.

Rigaku has collaborated with users in academia and industry to develop a family of X-ray diffractometers (such as the machines shown in Figure 5) that provide the most technologically advanced, versatile, and cost-effective means of judging the crystallinity of substances today. The machine used in this experiment.

**Fig.5** X-Ray Diffraction (XRD)

To analyze the composition and phases of geopolymers, XRD with Cu-Kα radiation (0.15418nm) were applied with scan angles in the range of 10-60 degrees.

### 3.2.4 TG-DTA

TG-DTA measures the weight change of the sample based on the temperature change of the sample and reference sample. For the program of simultaneous measurements TG and DTA, which is to measure the temperature change between the target sample and the reference sample were carried out. It can measure the water content and ash content of the sample, and evaluate its chemical properties such as decomposition, oxidation, and heat resistance. It can also be used for testing (calculation of activation energy) and accelerated degradation testing (comparison of thermophysical properties before and after degradation) to further test the reaction rate.

TG: When the weight changes, the current flowing through the coil causes it to return to its original current. The current corresponds to the weight change, and the current fluctuation is the weight change. output.

DTA: The temperature measurement is performed with a thermocouple provided in the sample holder. The detected temperature difference is output as a DTA signal.

The device is characterized by a vertical differential thermal balance with small drift (drift: TG-DTA signal fluctuation caused by temperature rise), high sensitivity, and stable measurement at low and high temperatures. Gas replacement by vacuum replacement (Residual oxygen has less influence on the measurement.) As shown in Figure 6.

In this thesis, the sample was heated to 1000°C by TG-DTA, and the dehydration state of the sample was analyzed.


**Fig.6** TG-DTA

### 3.2.5 Vickers hardness

Vickers hardness is a measure of a solid material's resistance to indentation. It is determined by calculation by pressing a diamond indentation into the sample surface under a specific load and by determining the size of the indentation, usually ranging from a few grams to several kilograms. The Vickers hardness value is obtained by measuring the size of the indentation remaining on the surface of the sample.

The instrument used in this paper is shown in Figure 7.

Vickers indenter was loaded at 1 kgf for 15 s with 12 points on the sample in this thesis.


**Fig.7 Vickers hardness equipment**

### 3.2.6 Electron irradiation

"ETIGO-III" is an inductively pulsed electron beam accelerator (the details of the confations is 8 MV, 5 kA and 30 ns). As shown in Figure 8, the accelerator includes 4 sensing units. Every acceleration cell with three amorphous iron cores is powered by the output voltage of the pulse forming line (670 kV). Each cell obtains an output voltage of 2 MV with a total output of 8 MV,

5 kA, and 30 ns. In this thesis, the potassium and metakaolin-based geopolymer was irradiated by ETIGO-Ⅲ at a peak voltage 2MeV, current 5kA and a pulse with of 100 ns.


**Fig.8** Linear Induction Accelerator, "ETIGO-III"

To further increase the absorbed dose of the sample, we used electron beam irradiation equipment at Takasaki Institute of Advanced Quantum Science operated at an acceleration voltage of 2 MeV. The absorbed dose reached about 1000kGy. The equipment is shown in Figure 9.

**Fig.9** Electron irradiation in the Cockcroft Walton accelerator

# 4 Pore-forming process in dehydration of potassium and metakaolin based geopolymer.

## 4.1 Research purpose

The passive autocatalytic recombiner (PAR) is widely used today. It is a device that removes hydrogen from a nuclear power plant containment in the event of an accident. The purpose is to prevent hydrogen explosions. Once the hydrogen concentration increases, the recombiner functions spontaneously. PARs are passive devices since they do not require other energy from the outside to operate. [60]

Hydrogen and oxygen molecules react chemically on the surface of the catalyst in an environment of low temperature and low hydrogen concentration. The chemical reaction produced steam. For Fukushima Daiichi Nuclear Power Station accident, many PARs are required in radioactive slurry vessels. It is required to produce catalysts supports at low costs. For PAE applications various excellent properties of geopolymers have been proposed as catalyst support materials. Considering the addition of the alkali solution in the synthetic original material of geopolymer, it is inevitable that geopolymers contain water. In previous research, the effects of humidity poisoning were very sensitive to metals such as Pd, Pt. The water molecules formed after the composite reaction of hydrogen and oxygen cover the surface of the catalyst, thus affecting the activity of the catalyst, and both alumina-supported catalysts and silica-supported catalysts are affected by deactivation to a certain extent [61]. Considering the inhibitory effect of water on catalysts, it is important to control the water content in the catalyst support.

Based on some studies, the porosity and pore size distribution in the geopolymer framework were tailored by simple synthetic condition changes [62]. Geopolymers inevitably contain pores, through which the permeation of foreign substances through the pore network can occur, which may degrade the mechanical properties.

Therefore, the aim of this chapter is to investigate the effect of dehydration of geopolymers on the pore distribution.

## 4.2 Experiments

This study is based on the research of Ms. Le Thi Chau Duyen. She investigated various Al: Si: K: $H_2O$ ratios. The geopolymer has good physical properties at the ratio of Al: Si: K: $H_2O$ is 1:2.1:0.8:8[63]. Therefore, this paper synthesized geopolymers with the same ratio (the composition of the samples as shown in Table 3).

**Table.3** composition of the samples

| Materials | $K_2O \cdot 2SiO_2$ | $H_2O$ | KOH | $SiO_2$ | $Al_2O_3 \cdot 2{\sim}3SiO_2$ | Total |
|---|---|---|---|---|---|---|
| Composition wt % | 28.12 | 25.38 | 5.11 | 10.95 | 30.43 | 100 |
| Ratio | **Al: Si : K :$H_2O$=1:2.1:0.8:8** | | | | | |

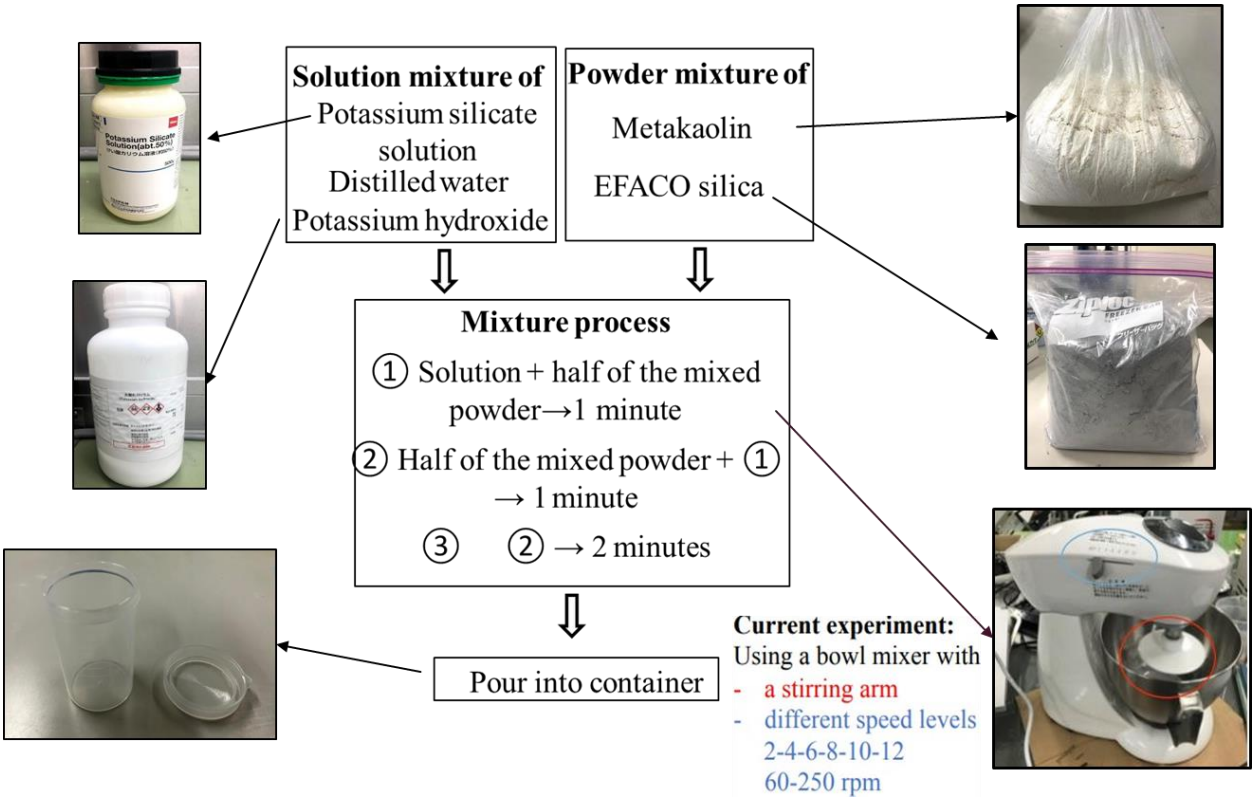


**Fig.10** Synthesis process of geopolymer samples.

Potassium hydroxide powder, distilled water and potassium silicate were mixed in proportions of 28.12wt%, 5.11wt%, and 25.38 wt%, respectively. The mixture was stirred until the powder was completely dissolved. The mixed solution was cooled down to room temperature for later use. Then 25.38wt.% EFACO silica powder and 30.43wt.% metakaolin were weighed for use.

In the mixing process, first we pour the prepared solution was poured into the stirring container, then add EFACO silica powder was added stirred for 1 minute at a stirring speed of 60rpm. For well mixing, half of the metakaolin was added into the slurry and then stir at 60rpm for about 2 minutes, after that, the other half of the metakaolin was added and stirred at the same speed for another 2 minutes. The last step, the slurry was mixed at approximately 80 rpm for about 5 min to

synthesize geopolymer samples. The mixing process is shown in Fig.10.


**Fig.11** The oven used in this research.

The slurry was poured into a mold after mixing. The mold used in this experiment is cylindrical, with a diameter of 33 mm and a height of 55 mm. In this experiment, 6 samples were synthesized with almost the same volume and mass and sealed with lids. The 6 samples were named with letters A-F and the geopolymer samples were segmented into three groups of 2 samples each (Group 1: Samples A and B; Group 2: Samples C and D; Group 3: Samples E and F). The three groups of samples were placed in the oven as shown in Fig. 11. The oven temperature was set at 60°C, the curing time was 4 days, for well explanation named this curing step as Curing 1. After four days, the three groups of samples were transferred to room temperature, 60°C and 80°C and stored until the 28th day. One sample in each group was completely demolded (Samples A, C, and E), while the other sample was uncapped but kept in the mold (Samples B, D, and F), we named this curing step as Curing 2. And the curing process in this experiment is shown in Table 4.

After the curing, the sample size was measured by a caliper to calculate the shrinkage.

***Table 4.*** The curing treatment processes

| Group number | Sample number | Curing 1 | | Curing 2 | | |
|---|---|---|---|---|---|---|
| | | Temperature | Time | Treatment | Temperature | Time |
| 1 | A | 60°C | 4 days | Demold | RT | 28 days |
| | B | | | Open cap | | |
| 2 | C | | | Demold | 60°C | |
| | D | | | Open cap | | |
| 3 | E | | | Demold | 80°C | |
| | F | | | Open cap | | |

## 4.3 Results

### 4.3.1 The body of geopolymer samples observations

The morphology of the 6 samples are shown in Fig. 12 after 28 days of curing completed. All of samples were kept in 60°C for 4 days (Curing 1). In Curing 2, Samples B, D, and F were stored without lid at room temperature (25ºC), 60ºC and 80ºC respectively until 28th days. Samples A, C, and E were completely demolded and stored at room temperature (25ºC), 60ºC and 80ºC, respectively until 28th days.

As shown in Fig.12, in curing 2, there is almost no cracks on Samples A and B cured at room temperature. However, Samples C, D, E, and F showed more cracks. In this experiment, cracks are easy to occur at high temperatures, and curing in the mold is beneficial to reduce the generation of cracks.

| Curing 2 condition | Sample A RT without case | Sample B RT with case | Sample C 60°C without case | Sample D 60°C with case | Sample E 80°C without case | Sample F 80°C with case |
|---|---|---|---|---|---|---|
| Samples body after 28 days |  |  |  |  |  |  |

***Fig. 12.*** Samples body observation

### 4.3.2 The shrinkage of geopolymer samples

The shrinkage of the 3 samples: Samples A, Samples C and Samples E were calculated. The results are shown in Table 5. The shrinkage increased with the temperature increase in Curing 2.

Table.5 The shrinkage situation of Samples A, C and E

| Sample number | After 4 days pre-cured at 60℃ The volume ($mm^3$) | After 28 days The volume ($mm^3$) | Shrinkage (%) |
|---|---|---|---|
| A | $4.43x10^4$ | $4.34x10^4$ | 2.13% |
| C | $4.43x10^4$ | $4.18x10^4$ | 5.64% |
| E | $5.08x10^4$ | $3.98x10^4$ | 21.65% |

### 4.3.3 Water content measurements

The samples were no longer closed after Curing 1 (4 days). This causes the samples to lose water, which then changes in weight. Body weight changes were recorded during curring 2 from day 4 to day 28. From weight measurements to day 28, weight changes were plotted (relative weight loss during post-curing is shown). Weight loss accelerates as temperature rises.

The weight loss was due to dehydration. In this research, water content measurement depended on weight loss (the water content changed during post curing as shown in Fig.13)

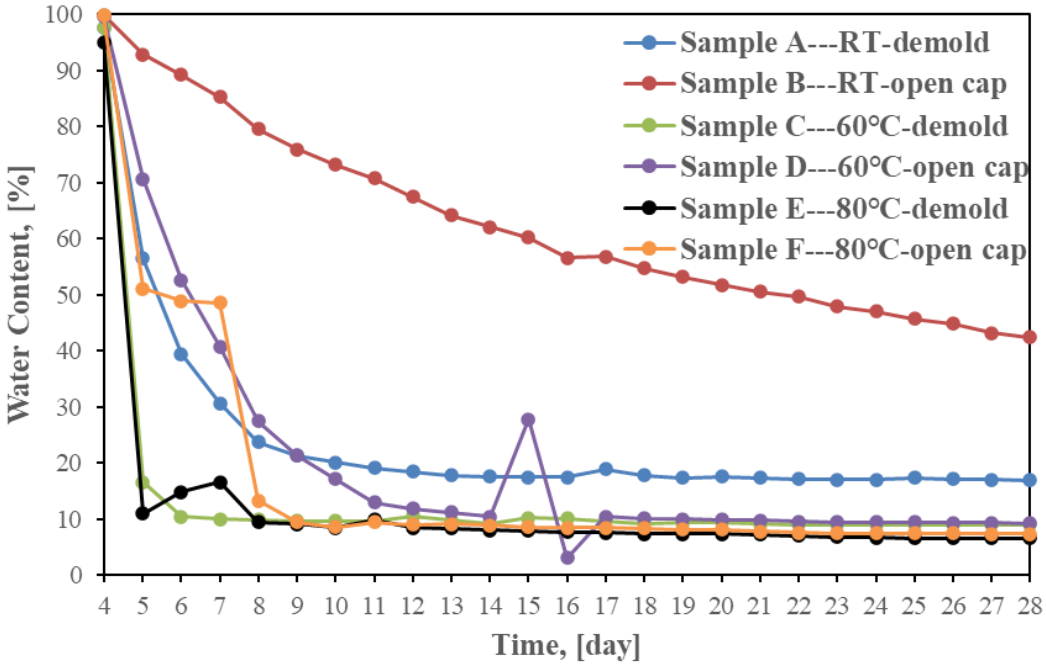


***Fig. 13.*** The water content changed during post curing.

### 4.3.4 The pore size measurement

In order not to double count the pores as much as possible, we took 50 images with SEM using the red path marked in Fig 14. In this way, the scanning field of the SEM almost covers the surface of the sample. At least 500 pore sizes were counted for each sample.

Images were taken at 50X magnification (images shown). As shown in the pore marked by double arrows, the diameter of a pore that was approximated by a circle was measured.

Finally, count the number of pores with a diameter range. The pore size distribution plot in Fig. 15 was made.

The pore size distribution in Figure 15 shows the same trend despite the difference in Curing 2 temperature. The average size of the pore for the demolded and open cap samples was almost the same as $1.52x10^2$ µm, $1.51x10^2$ µm and $1.33x10^2$ µm, $1.66\ x10^2$ µm, $1.60x10^2$ µm. Through these experiments, the pore size distributions of the geopolymer samples were almost the same.

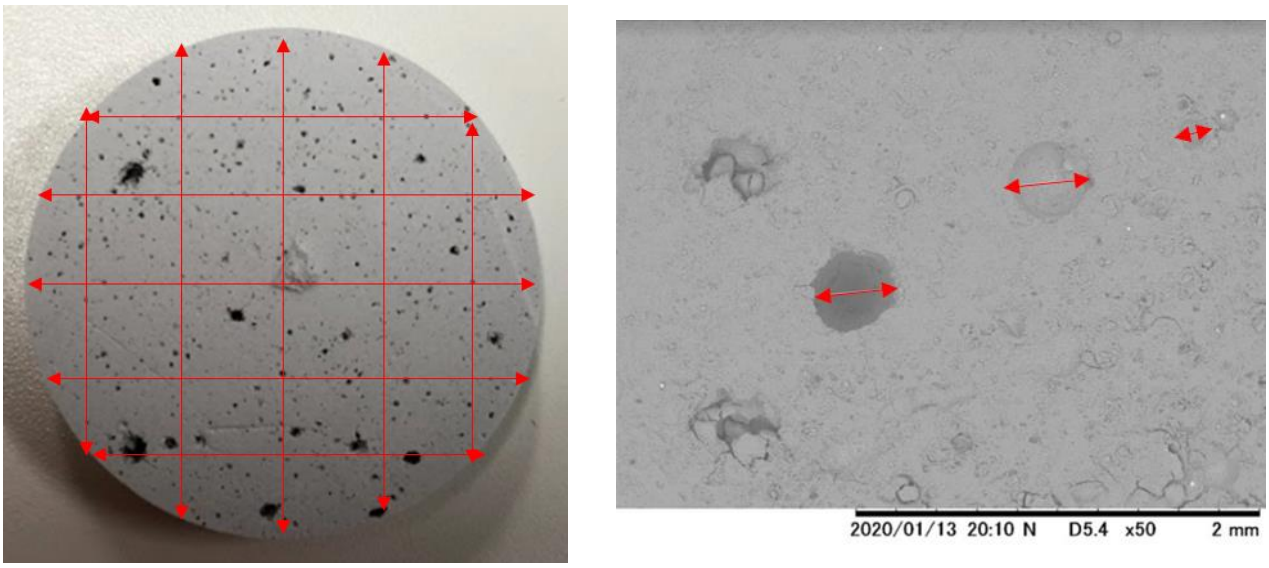


Fig.14 SEM

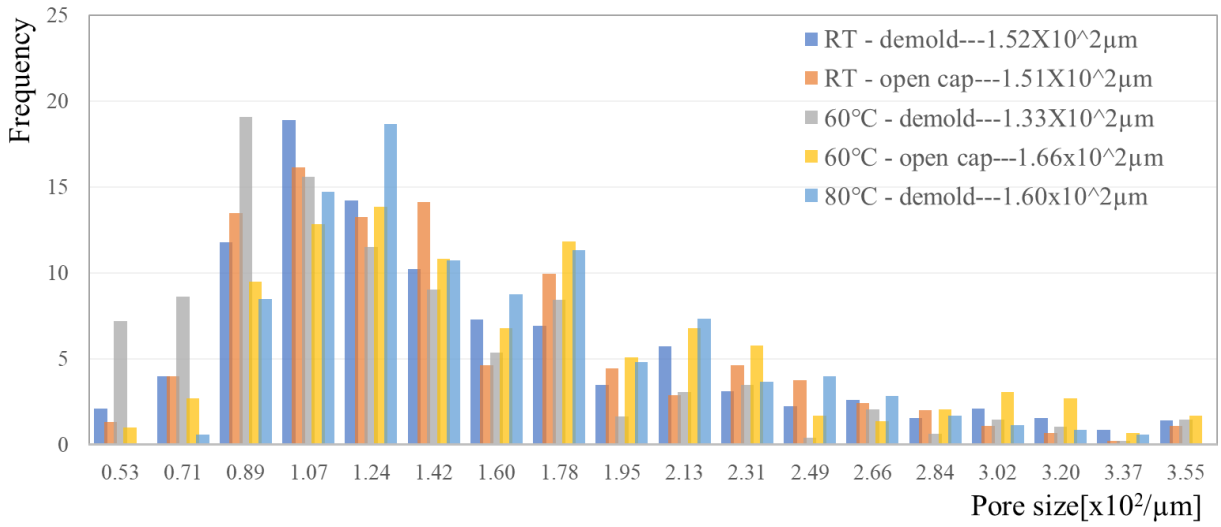


***Fig. 15***. Pore size distribution

### 4.3.5 TG-DTA measurements

As the heating rate increases, the small peak between 200 ℃ and 300 ℃ in TG-DTA shifts to the right. Some researchers showed that dehydration period can be extended when fast heat rates were applied, so peak between 200ºC and 300ºC should be water [64].

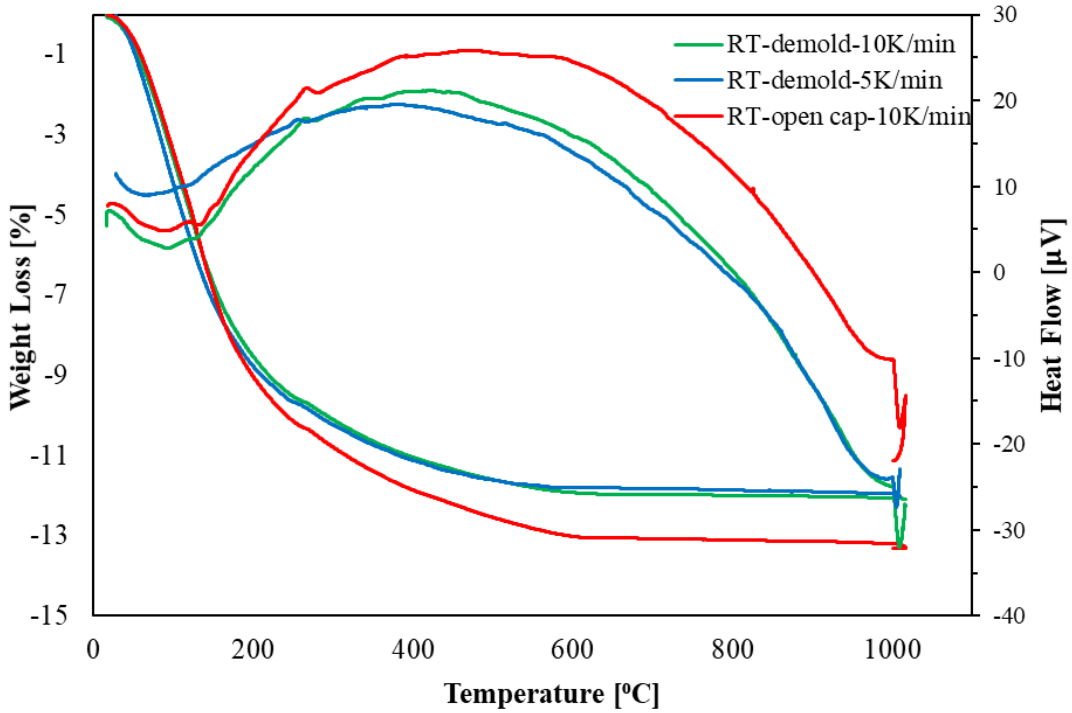


***Fig. 16.*** TG-DTA measurements of Samples A and B

### 4.3.6 XRD measurements

XRD patterns of the geopolymer samples after heating to various temperatures are shown in Fig.17.

At 200℃, the $TiO_2$ peaks were seen, it came from the metakaolin due to the impurities. Some small peaks for illite, andradite and $SiO_2$ were visible. But the broad peak near 30 degree was seen, which was different from the raw materials, such as metakaolin, and silica. It was for geopolymer. It also showed an amorphous state despite heating to 1000 ℃, which reflects the stability amorphous structure of the geopolymer. This result is explained by the difficulties of zeolite formation in potassium and metakaolin based geopolymer [65].

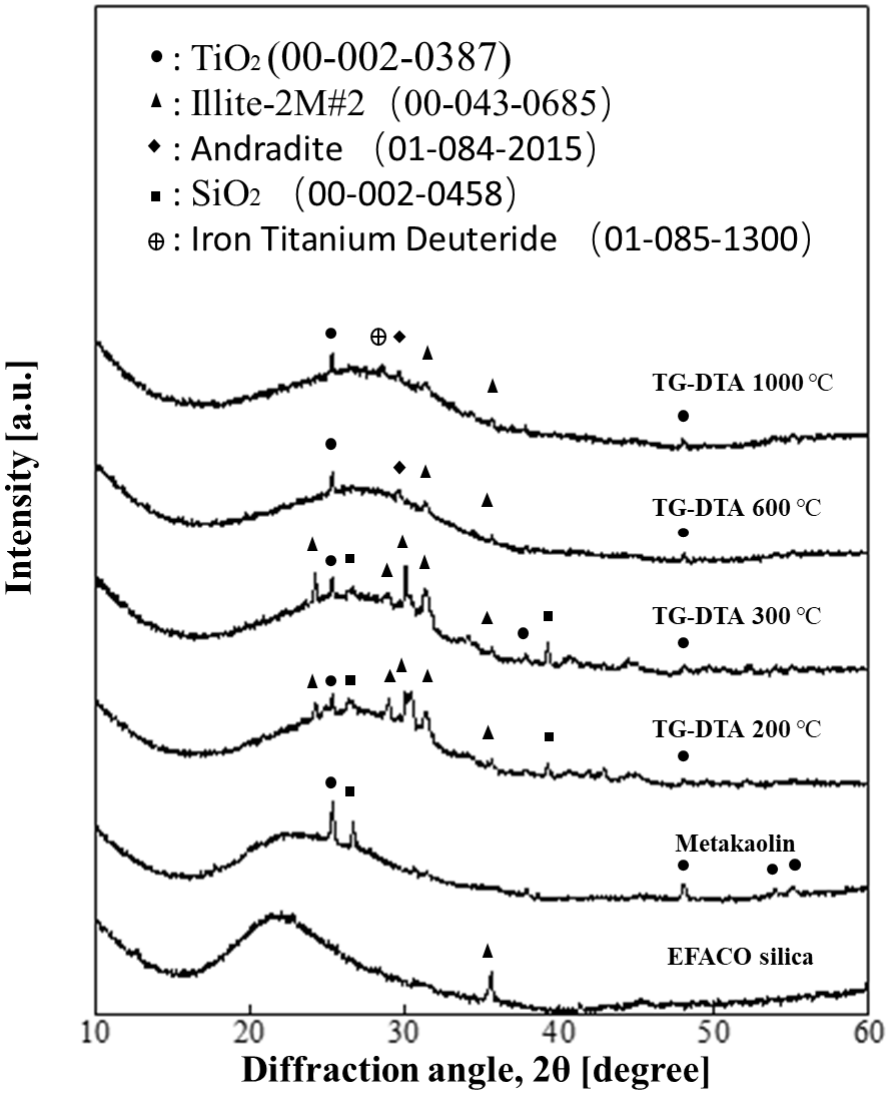


**Fig. 17.** XRD patterns of the geopolymer samples after heating to various temperature

## 4.4 Discussion

In this research, Curing 1 was performed at the same temperature for about 4 days and then samples were kept at different temperatures to continue Curing 2. The water content had been declining, and the cracking of the samples is relatively severe at relatively high temperatures (60°C and 80°C). But the average pores size was almost the same from 10μm to 20μm. As mentioned in the previous study, the pore size slightly increased with increasing curing temperature when other conditions were the same [66]. From this study, we could infer that the pores size was formed steadily for at least the first four days.

It can be inferred from this research that at high temperatures, most of the reason for the accelerated loss of water may depend on the open channels. The previous research [67] showed that evaporation of water and loss of bound water in geopolymers lead to reorganization of aluminosilicates at high temperatures, which may lead to shrinkage around the pores, which leads to microcracks, which in turn produce open channels. Open channels speed up the passage and release of water.

The pressure inside a pore is inversely proportional to the pore radius, and directly proportional to the surface tension (possibly related to viscosity) in a liquid as shown in the formular [68].

**At equilibrium, the pressure difference between the inside and outside of the pore is obtained from the Helmholtz equation:**

$$P_g - P_l = \frac{2\sigma}{r}.$$

In the formula: $P_g$ is the internal pressure of the pore; $P_l$ is the liquid pressure; σ is the surface tension coefficient of the gas-liquid interface; r is the radius of pore in liquid.

In this experiment, dehydration was expected to increase the viscosity [69]. The average pore size of the demolded (quick dehydration) and uncapped (slow dehydration) samples was almost the same. This means that the pores are formed at a certain viscosity and a single chemical reaction (dehydration) took place which was the origin of the pore formation.

The XRD pattern showed that when the sample was heated up to 1000 °C, some new crystal

phases such as garnet and iron-titanium-deuterium were produced in the sample, which indicated that the thermal stability of the sample might be improved. It showed that the samples were still containing water, which was inferred that the high temperature heating process caused the samples to form a more stable bond water.

## 4.5 Conclusions

Synthesis and the dehydration of potassium and metakaolin based geopolymer were conducted. Pore size distribution showed almost the same for the samples that cured at the same initial temperature for 4 days, then moved to different post curing condition. The pore size distribution was not affected by the following curing temperature. It was expected that the pore forming took place at the same viscosity.

Evaporation of water continued until approximately 300°C, at which point most of the free water was released. 90% of weight loss happened below 400°C. After 400°C, the bound water began to be released gradually, however, some part of the bound water still existed in the form of strong chemical bonds, and did not even release until 1000°C. The geopolymer samples did not crystallize.

# 5. Effect of dehydration time and air tightness on pore size distribution of potassium based geopolymer

## 5.1 Research purpose

It was shown in Chapter 4 that the pore size distribution was almost the same after being kept at 60°C for about 4 days, independent of the post-cure temperature. This means that pores may form within the first 4 days. because of the pore size distribution and porosity in geopolymers can affect their heat transfer, air circulation, etc. [70]. Air circulation may also affect the pore size distribution during curing. Therefore, in this study, the effects of dehydration time (from 1 to 4 days) and air tightness (with lid and without lid) on the pores size distribution of potassium and metakaolin based geopolymers will be investigated.

## 5.2 Experiments

In this experiment, 8 samples were synthesized in the same way as in the previous chapter. 8 samples were divided into 4 groups (Group1-4). One group contains 2 samples (Group 1: Samples A and B; Group 2: Samples C and D; Group 3: Samples E and F; Group 4: Samples G and H). The curing conditions as shown in Table 1. The curing process is also divided into 2 steps, Curing 1 and Curing 2. In Curing 1, 8 samples were airtightly dried at 60°C for different times from Group 1 to Group 4 and cured at 60°C for 1 to 4 days, respectively. In Curing 2, the 8 groups of samples were all transferred to room temperature, one of the samples in each group continued to cure with the lid on, and the other one opened the lid. In a previous study we learned that the geopolymer was almost completely dehydrated on the 14th day. So, in this chapter, Curing 2 will be until the 14th day.

Table. 6. The curing treatment processes

| Group number | Sample number | Curing 1 | | | Curing 2 | | |
|---|---|---|---|---|---|---|---|
| | | Temperature | Time | Treatment | Temperature | Time | Treatment |
| 1 | A | 60°C | 1 day | With lid | RT | 13 days | With lid |
| | B | | | | | | Open lid |
| 2 | C | | 2 days | | | 12 days | With lid |
| | D | | | | | | Open lid |
| 3 | E | | 3 days | | | 11 days | With lid |
| | F | | | | | | Open lid |
| 4 | G | | 4 days | | | 10 days | With lid |
| | H | | | | | | Open lid |

The ambient temperature was about 20° C. The relative humidity was 45%±5%.

## 5.3 Result

### 5.3.1 Water content measurement

The relative weight changes for the samples are shown in Fig 18. The figure shows the relative weight change of the sample that cured without lid in Curing 2. After Curing 1, the weight decreased suddenly within 2 days. The relative weight changes of all samples were around 10% until the 14th day and were not significant variations.

The shrinkage was obtained by measuring the volume on day 14 and the initial volume when the geopolymer samples were synthesized. The results showed that the samples cured with lid in Curing 2, the shrinkage of the samples at day 14 was almost consistent at about 0.5%. For the sample in Curing 2 without lid, the shrinkage of the samples cured at 60°C in Curing 1 for 1-4 days were 2.2% (Samples B), 2.2% (Samples D), 2.1% (Samples F) and 2.1% (Samples H), respectively, it was not so much different.

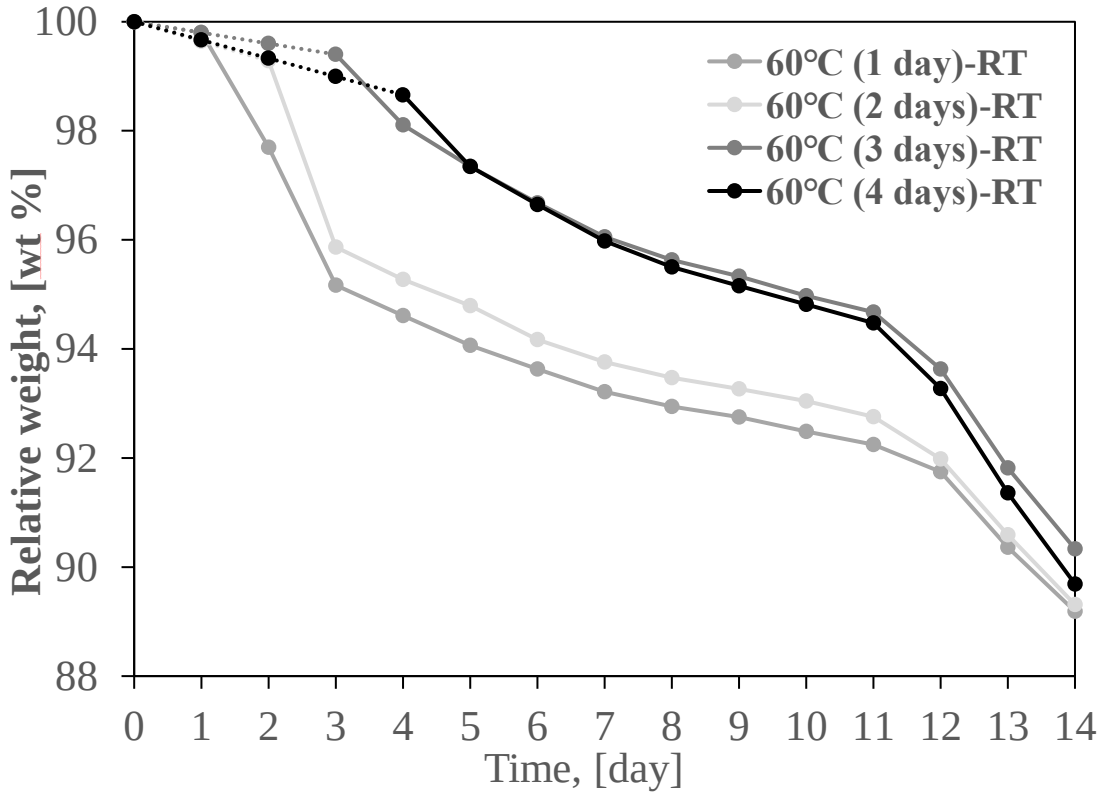


***Fig. 18.*** The relative weight decreases during the various the different post curing conditions.

### 5.3.2 SEM measurement

SEM images of the geopolymer samples with different curing times in Curing 1 are shown in Fig. 19. When the sample was kept at 60 °C for about 1 day, the SEM images showed a slightly larger porosity than the other samples. Increased curing time may have the potential to form larger pores.

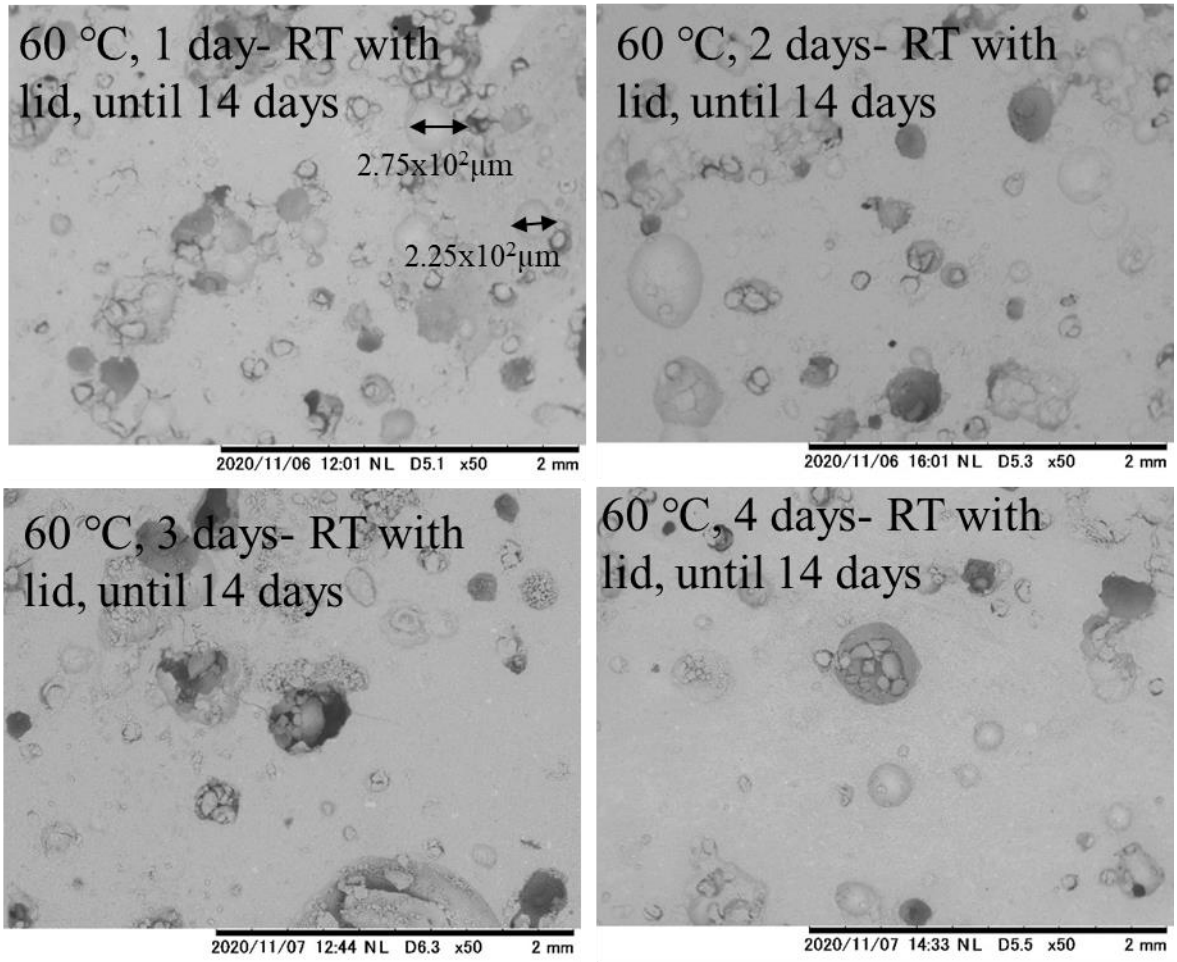


**Fig.19. SEM images.**

### 5.3.3 Pore size distribution measurement

The pore size distribution is shown in Figs. 20 - 23. In Fig 20 and 21 when the samples were kept at 60°C for the same period, there was a slight difference in average pore size for the lidded and unlidded samples. However, for the unlidded samples, the average pore size ranged from 1.4 × $10^2$µm to 2.3 × $10^2$µm, and for the lidded samples, the average pore size mainly distributed between 0.9 × $10^2$µm to 2.0 × $10^2$µm. The average pore size of covered samples is smaller than

that of lidded samples. In Figs 22 and 23 the pore sizes at the upper and bottom are mainly distributed between $1.1\times10^2$μm and $2.5\times10^2$μm. However, in the range from $1.6 \times 10^2$μm to $2.0 \times 10^2$μm, the frequency of the upper pore size distribution is significantly larger than that of the bottom about 21%. The longer the time in Curing 1, pore size tends to be larger. This is like the result that was observed in SEM images in Fig. 19.

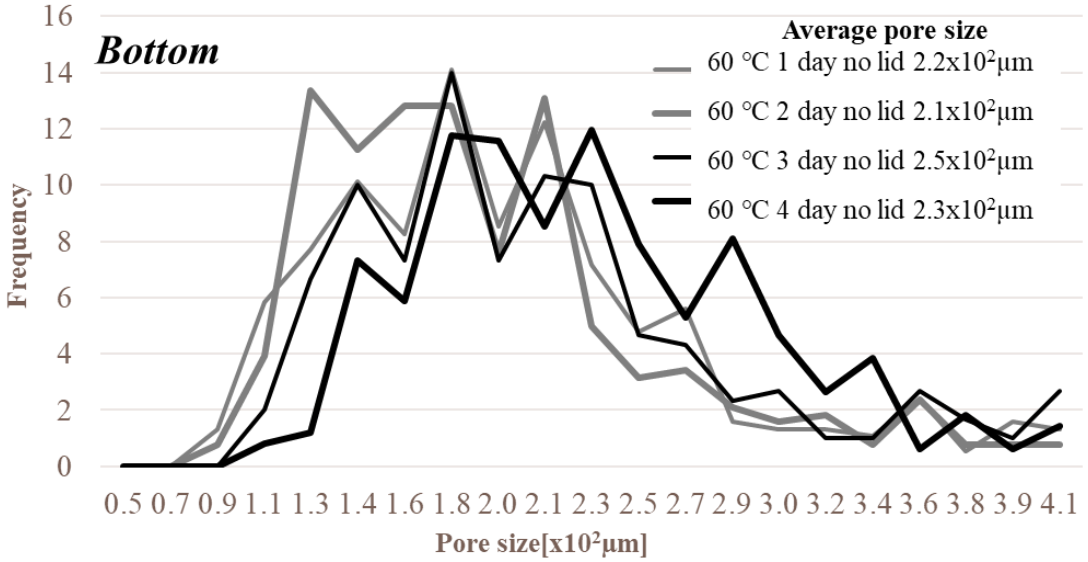


**(a)**

***Fig. 20.*** Pore size distribution for the sample cured no lid.

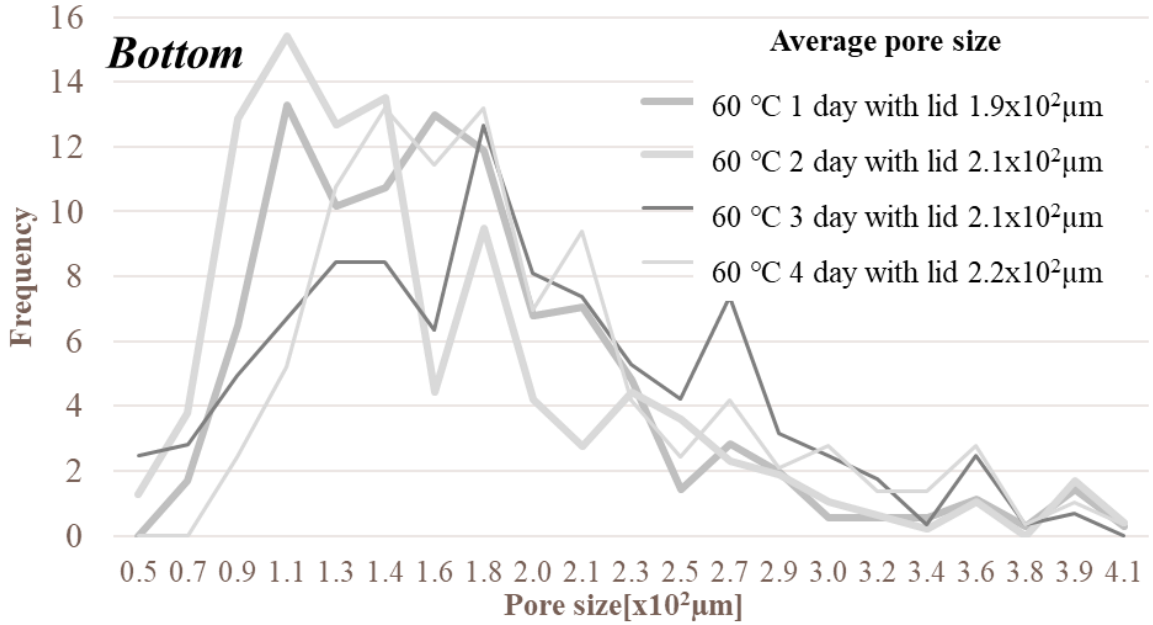


**(b)**

***Fig. 21.*** Pore size distribution for the sample cured with lid.

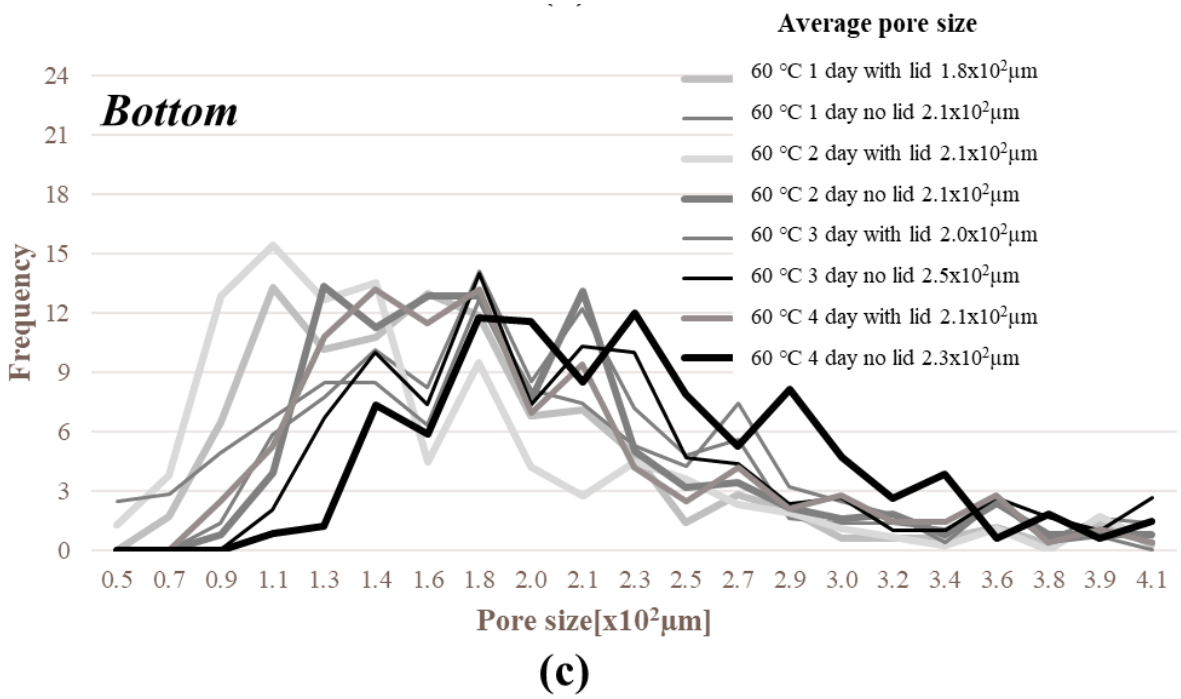


**(c)**

***Fig. 22.*** The pore size distribution for the bottom

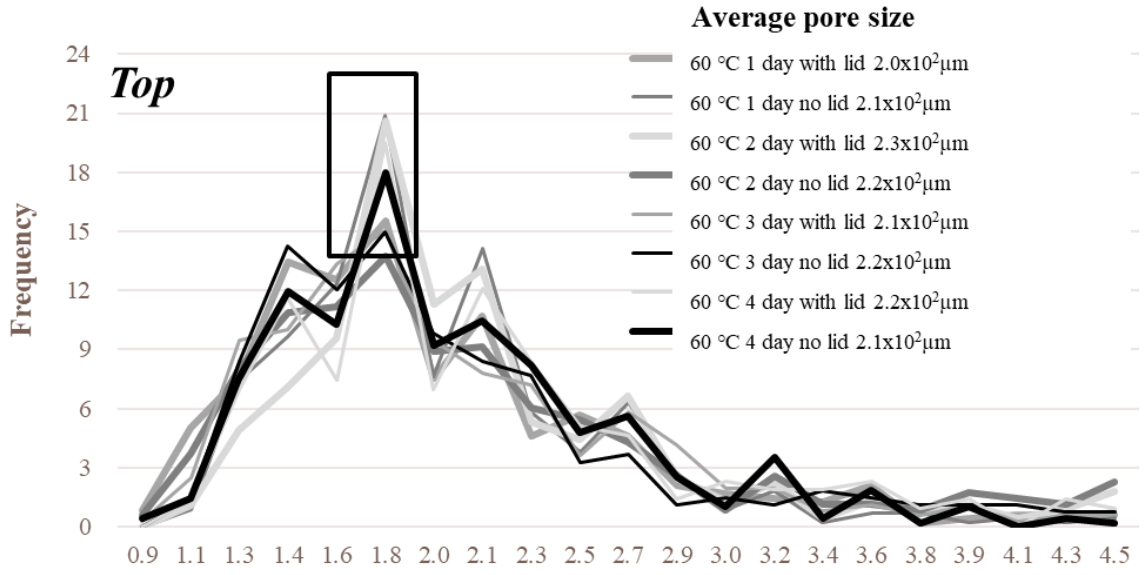


**(d)**

Fig. 23. The pore size distribution for the top

### 5.3.4 XRD measurement

The XRD pattern as shown in Fig. 24 and there are more peaks for the samples cured with the lid compared to the samples cured without the lid. Although there are some crystalline peaks, the broad peaks are still at the same position, so the same geopolymer was synthesized.

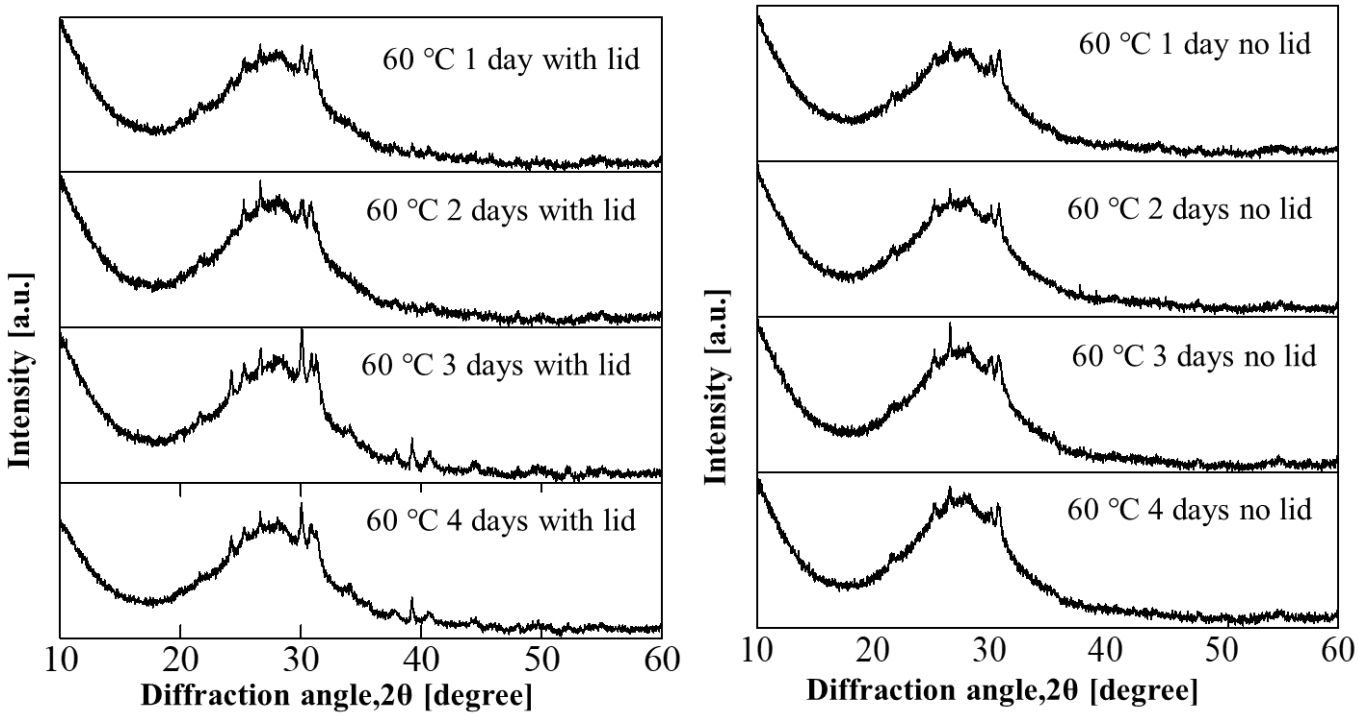


**Fig.24** X-Ray Diffraction (XRD)

### 5.3.5 Vickers hardness measurement

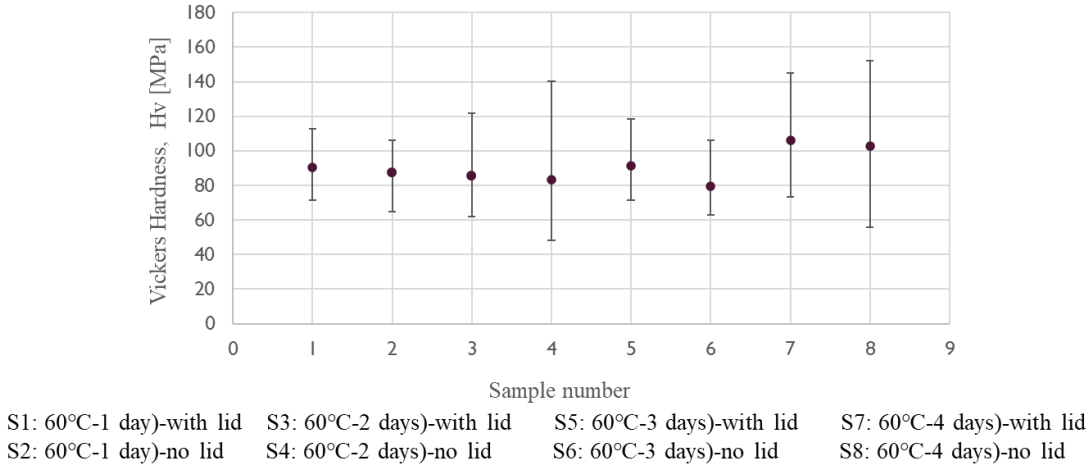


**Fig. 25** The Vickers hardness

The Vickers hardness as shown in Figure 25, and the error bars for each sample to indicate the variations of hardness values are also instated. By the increase of curing time, the average Vickers

hardness did not change much. Even though the sample was kept at 60°C for just 1 day, the Vickers hardness had reached a higher value on the 14th day.

### 5.4 Discussion

In this experiment, the relative weight loss at day 14 was similar at around 10% for all metakaolin and potassium-based geopolymers and was not affected by the curing time in Curing 1. It was concluded that the samples might have formed similar microstructures in Curing 1 and were not affected by the curing time.

XRD pattern also shows that similar amorphous structures of geopolymers are formed around 27°C, confirming similar microstructures and similar dehydration amounts mentioned earlier.

SEM images show that long time curing may reduce the porosity slightly, while short time curing has a larger number of small pores.

The pore size distribution plots in Fig. 20 and Fig. 21 showed that there was a high frequency of small pores in the samples with the shorter curing time in Cure 1, regardless of whether the samples were sealed. However, the average pore diameter did not change much.

The pore size distributions in Fig. 22 and Fig. 23 showed that the pore size tends to be smaller at the bottom relative to the top. Fig. 22 showed that the pores at the bottom tend to become larger as the curing time increased in Curing 1. However, the average pore size properties were almost the same and the Vickers hardness of the geopolymer samples was not so much different. This study shows that geopolymers can reach a high value of about 90 MPa in Vickers hardness within 1 day.

### 5.5 Conclusions

In this chapter, the synthesis and dehydration of potassium and metakaolin based geopolymers were conducted. The pore size distribution and Vickers hardness of geopolymers under different curing time and air tightness conditions were studied.

This study showed that when samples were cured at 60 °C for from 1 to 4 days and subsequently changed to airtightness, the shrinkage remained almost consistent at around 2.1%. It was concluded that potassium and metakaolin based geopolymers formed stably at an early cure of 1 day. The Vickers hardness of the sample kept at 60°C for 1 day and the Vickers hardness value on the 14th day after curing at 60°C for four days were not significantly enhanced. This property is beneficial to reduce the hardness in practical industrial applications and the prediction costs.

The results of pore size distribution tend to be larger at the top compared to the bottom. As the pre-curing time increased, the pore size distribution at the bottom tended to large pores, while the pore distribution at the top showed greater consistency. However, the average pore size was almost the same for all samples, about $2.1 \times 10^2$μm. According to this result, the pore size distribution can be controlled by controlling the early curing time for practical industrial applications.

# 6. The influence of electron irradiation on the mechanical properties of potassium and metakaolin based geopolymer

### 6.1 Research purpose

In the previous study, the effect of curing temperature and curing time on the pores size distribution was investigated. It was concluded that the pores of geopolymers could be formed stably in one day. The Vickers hardness has reached a relatively high level.

Therefore, in this chapter, the research on pore size distribution by changing the water content of the geopolymer is conducted to use the geopolymer for the application of compacting radioactive aluminum ions.

### 6.2 Experiments

Geopolymer samples were synthesized by mixing potassium silicate, potassium hydroxide powder and distilled water. (4 types of geopolymer samples were synthesized with the ratio of Al: Si: K: $H_2O$=1:2.1:0.8:7,8,9 10 respectively).

Step 1 the solution was mixed until the powder was completely dissolved. Then, the solution was cooled down to room temperature.

Step 2, EFACO silica powder was added with solution, and stirred at a speed of 60rpm for 1 minute, then add metakaolin 2 times, mixed at a speed of 60rpm for 2 minutes each time. Finally, the slurry was mixed at approximately 80 rpm for 5 min to synthesize geopolymer samples.

Table.7 composition of the samples

| **Raw Materials** | $K_2O \cdot 2SiO_2$ | $H_2O$ | KOH | $SiO_2$ | $Al_2O_3 \cdot 2{\sim}3SiO_2$ |
|---|---|---|---|---|---|
| **Al: Si : K :$H_2O$ = 1:2.1:0.8:7<br>1:2.1:0.8:8<br>1:2.1:0.8:9<br>1:2.1:0.8:10** | | | | | |

Table.8. The curing treatment processes.

| **Curing 1** | | | **Curing 2** | | |
|---|---|---|---|---|---|
| **Temperature** | **Time** | **Treatment** | **Temperature** | **Time** | **Treatment** |
| **RT** | **1 day** | **With lid** | **RT** | **6 days** | **Without lid** |
| **40°C** | | | | | |
| **60°C** | | | | | |

Samples were kept at RT, 40°C and 60°C with lid for 1 days (Curing 1) respectively. Then, samples were further kept at RT without lid until 7 days. The curing treatment conditions are shown in Table 7.

## 6.3 Results

### 6.3.1 Water content

The weight change for each sample was recorded every day so that the water content could be calculated during the whole process. The results are shown in Figs 26-28. When the temperature was the same, the relative weight decreased more with the water content increase. The range of relative weight decrease was from 10% to 14%).

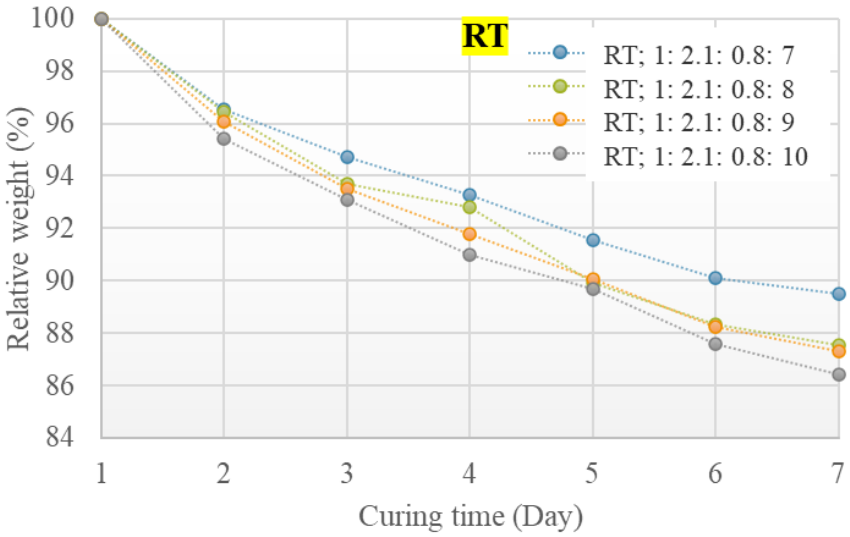


Fig. 26 relative weight change during curing at RT

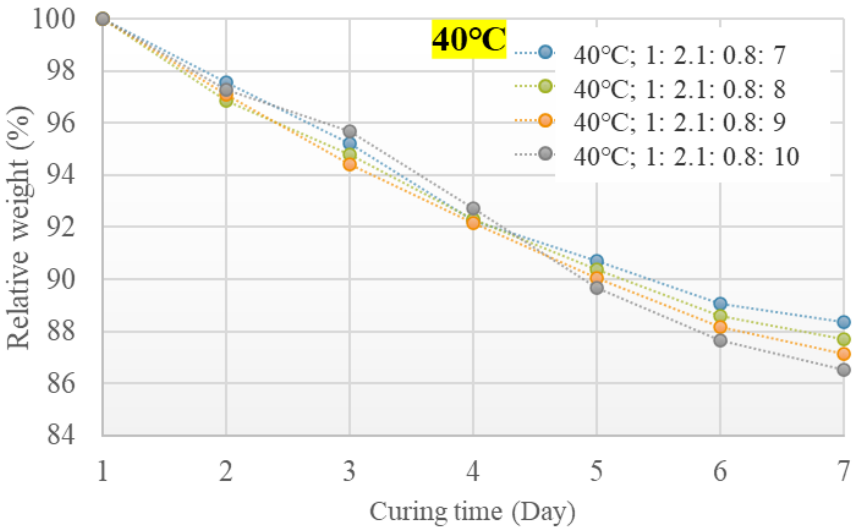


Fig. 27 relative weight change during curing at 40°C

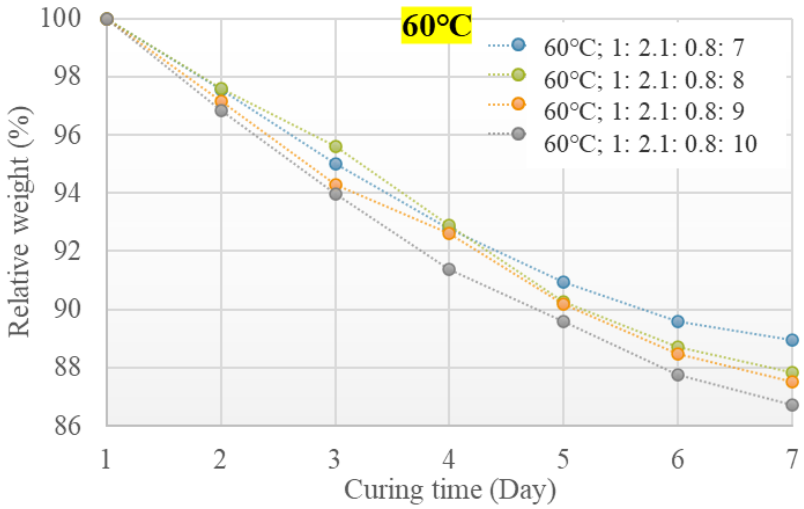


Fig. 28 relative weight change during curing at 60°C

### 6.3.2 SEM

Using SEM to observe the cross-section at 5 mm from the bottom pictures of nearly 50 pictures for each sample. Some of them are shown in Figs 29-30. From the pictures, statistics on the pores and plot the pore size distribution were obtained. For the samples were cured at room temperature (Fig. 29), 40°C (Fig. 30), and 60°C (Fig. 31), as the water content increases, the surface damage phenomenon gradually intensifies.

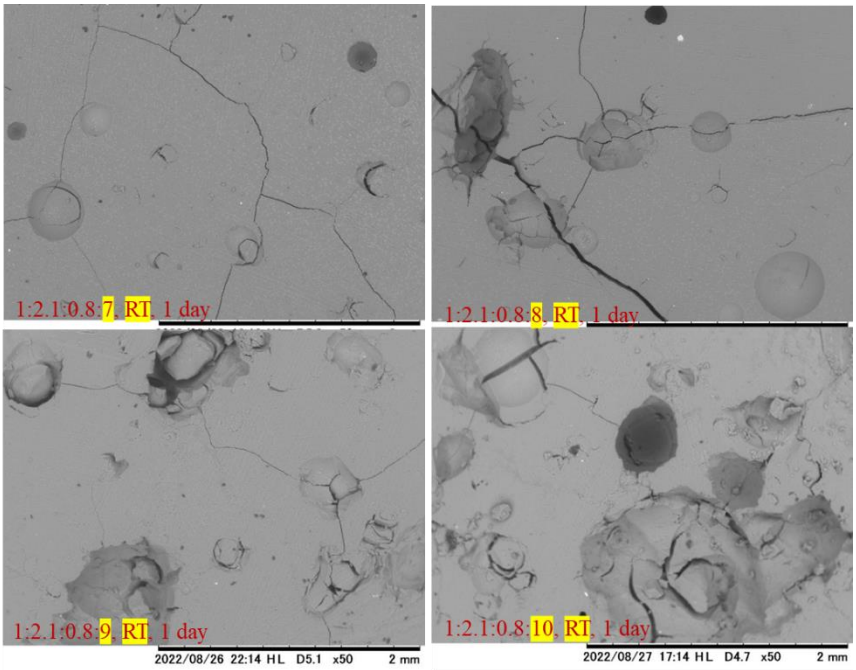


Fig. 29 SEM of the sample curing at RT

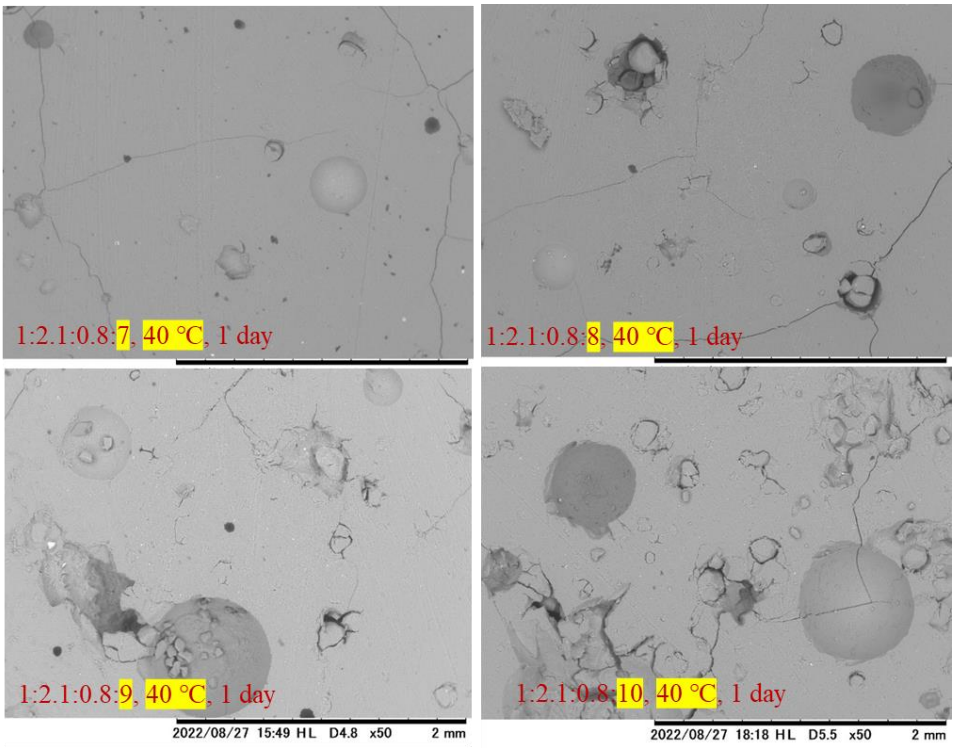


Fig. 30 SEM of the sample curing at 40°C

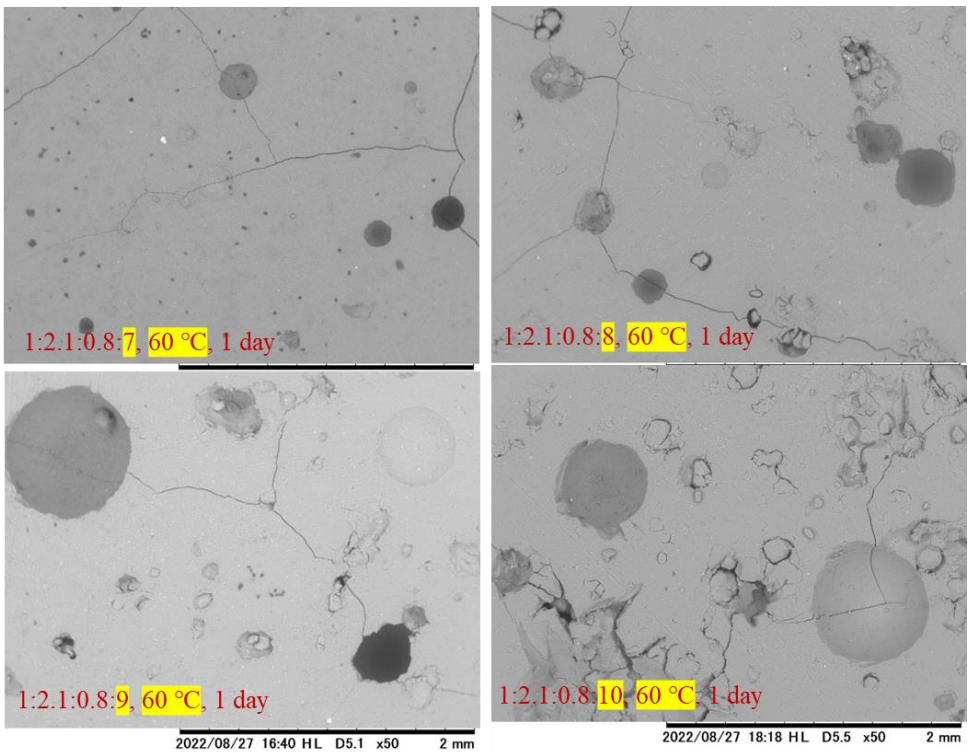


Fig. 31 SEM of the sample curing at 60°C

### 6.3.3 **Pore size distribution**

Pore size distributions are shown in Figs 32- 38. When the curing temperature is the same (Figs 32- 38). With the water content increasing, the average pore size showed a slight increase. With the same water content (1:2.1:0.8:8,9,10) (Figs 35- 38), the average pore size showed a decrease

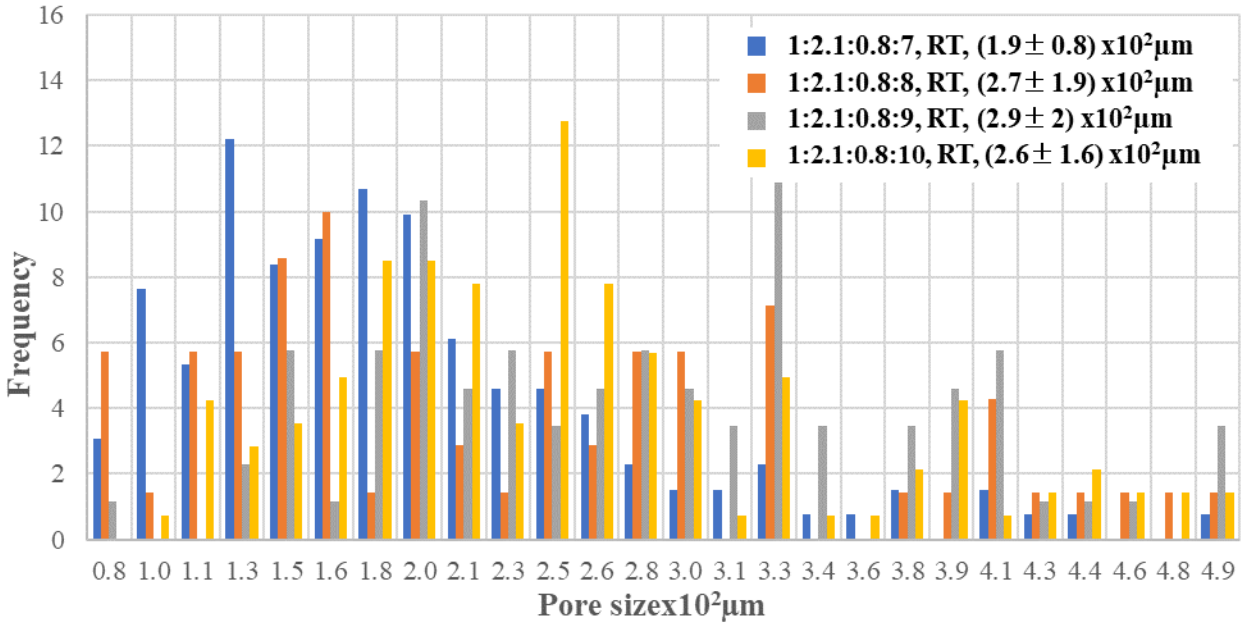


with the curing temperature increase.

Fig. 32 Pore size distribution of the sample curing at RT

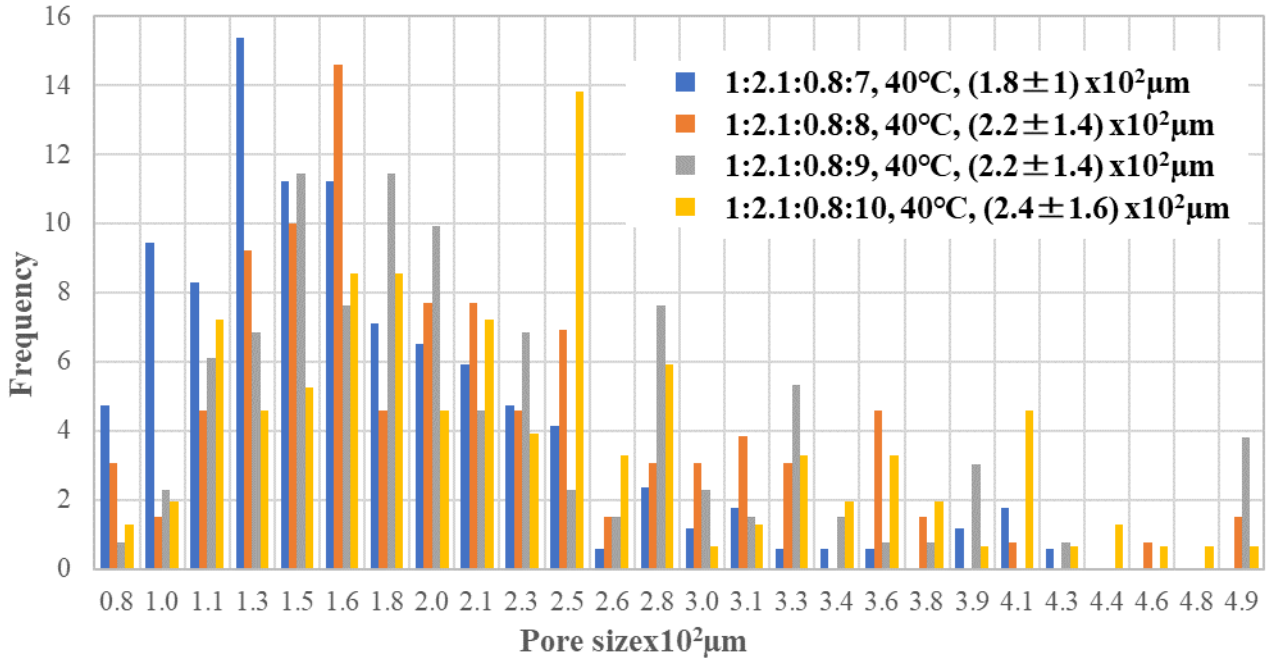


Fig. 33 Pore size distribution of the sample curing at 40°C

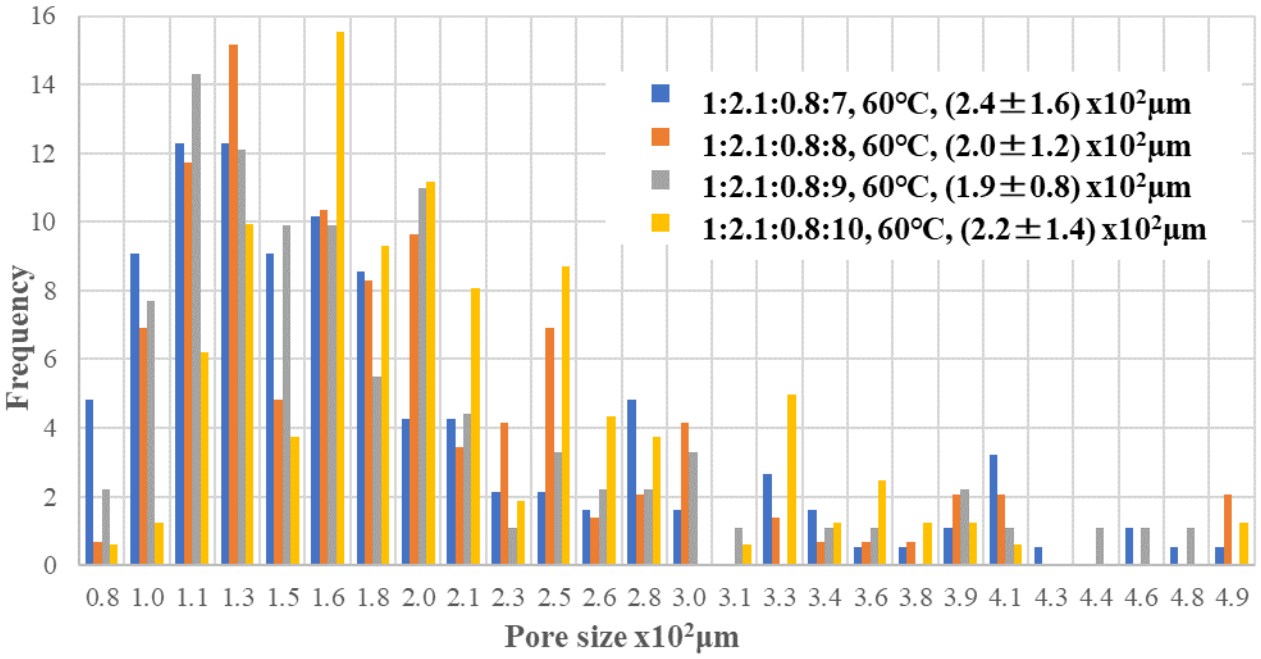


Fig. 34 Pore size distribution of the sample curing at 60°C

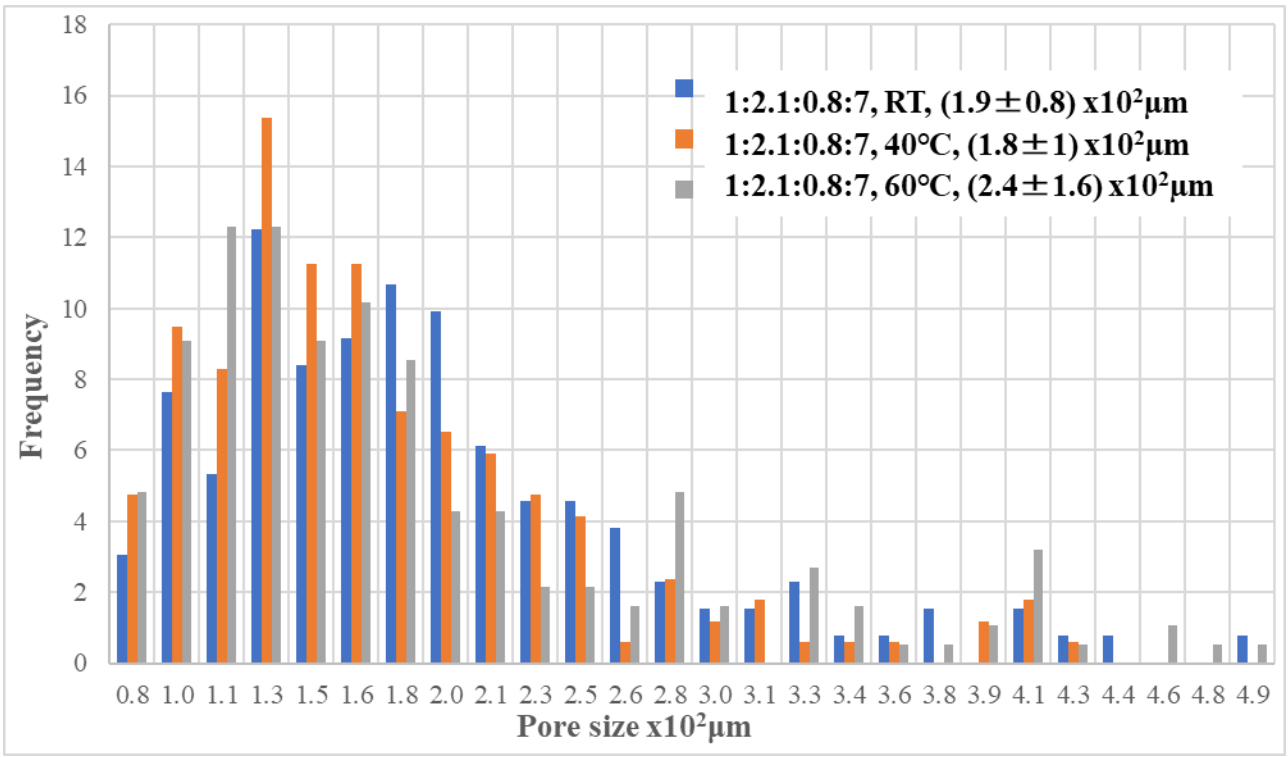


Fig. 35 Pore size distribution of the sample with the water ratio of 7

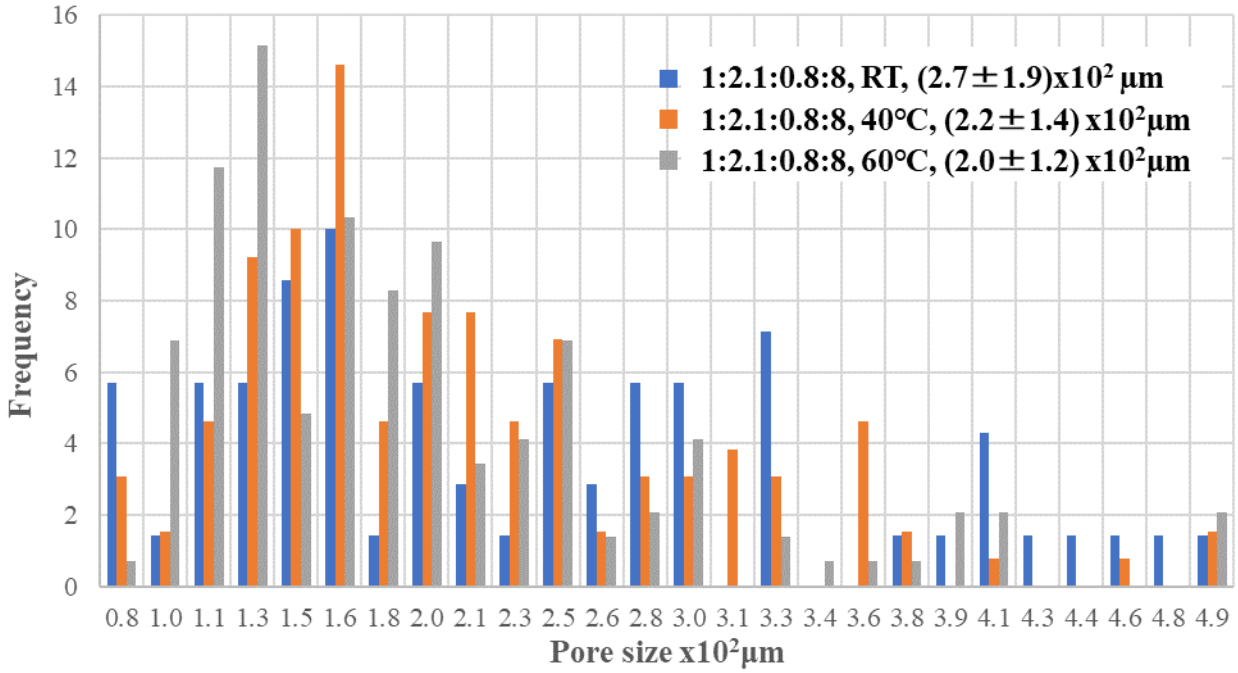


Fig. 36 Pore size distribution of the sample with the water ratio of 8

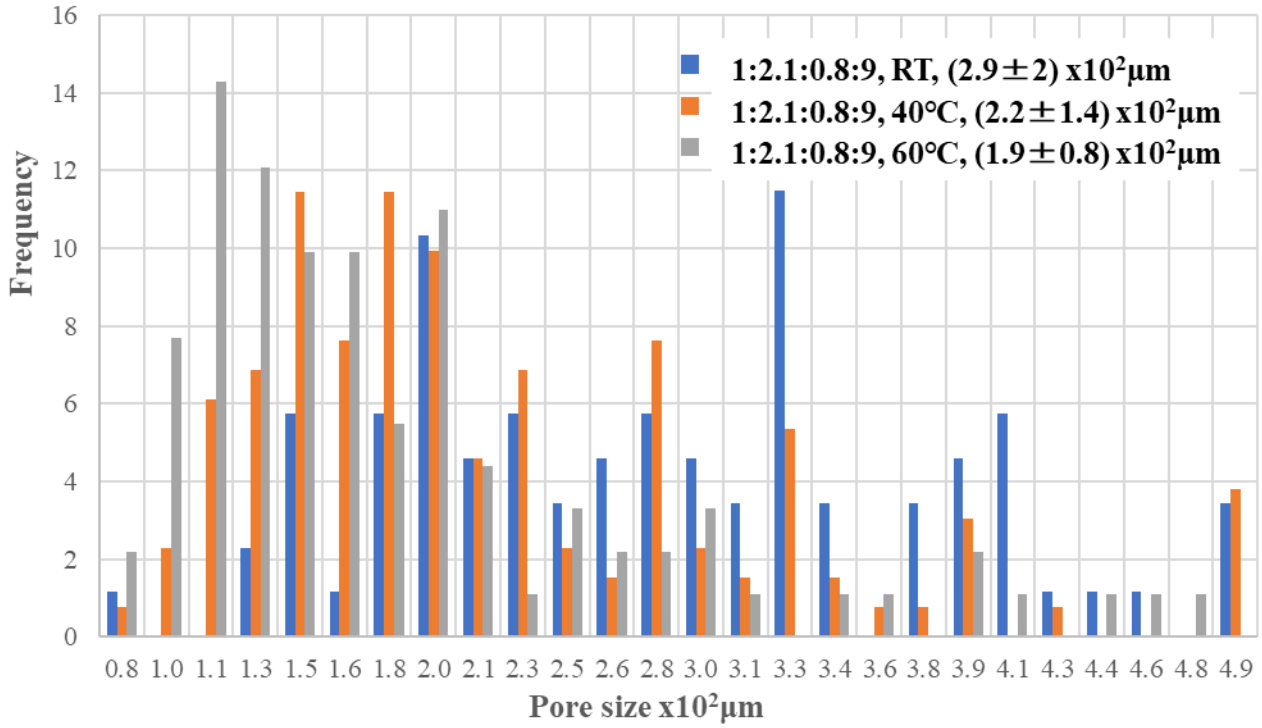


Fig. 37 Pore size distribution of the sample with the water ratio of 9

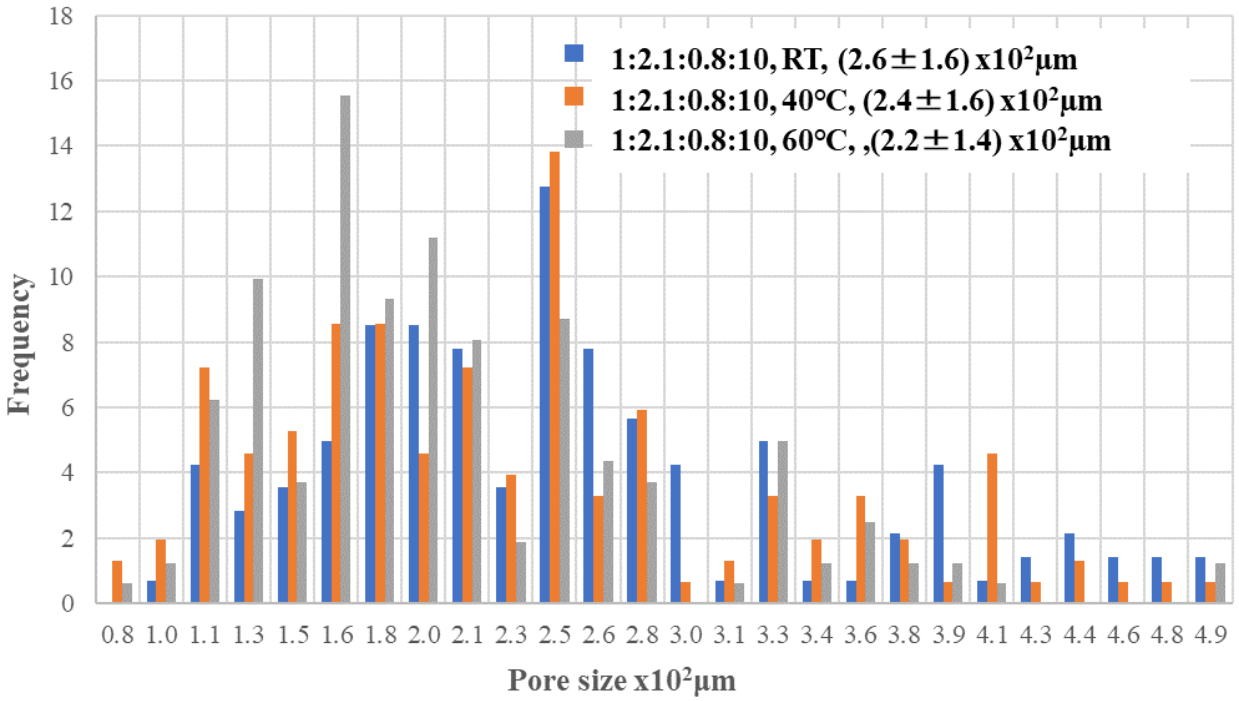


Fig. 38 Pore size distribution of the sample with the water ratio of 10

### 6.3.4 Vickers hardness measurement

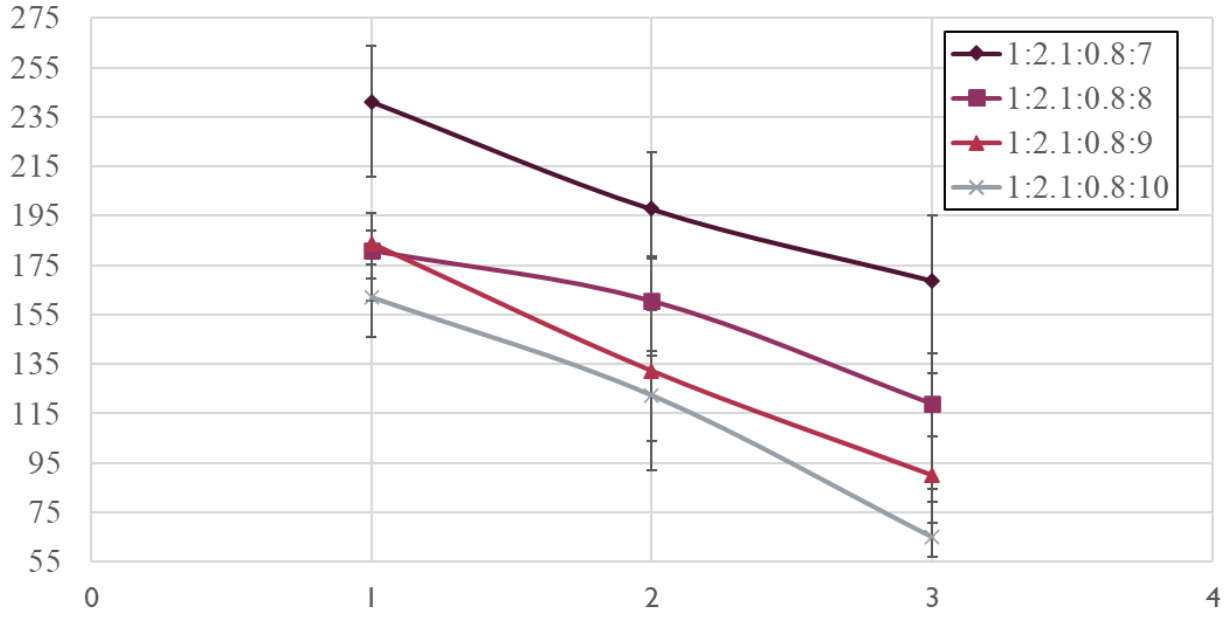


***Fig 39.* Vickers hardness**

Before the hardness test, we grind the test surface until the surface of the sample is as smooth

as a mirror (to clearly observe the indentation), and then we set the force of the indentation to 1kgf to test the hardness of the sample. With the water content increase, the Vickers hardness decrease.

### 6.3.5 Electron irradiation measurement

The potassium and metakaolin-based geopolymer samples were irradiated by ETIGO-III at a peak voltage 2MeV, current 5kA and a pulse with of 100 ns. Continuous electron beam irradiation up to 1000kGy was also carried out in this experiment by a Cockcroft-Walton accelerator at National Institute Quarter Science and Technology. Fig. 40 shows the target installation diagram. Irradiation test on the surface of geopolymer to observe the surface change before and after different shots. This time, four shots were applied, and the number of shots times will be varied for each sample.

Each sample was cut into 4 pieces, and then the sample was fixed on an acrylic plate as shown in Fig. 40. Each group of samples consisted of four samples with different water contents. Each sample was covered with a filter dosimeter. After the first shot, a group of samples and the dosemeter in the upper left corner was tale out. Then after the second shots, another group was taken out after each shot. After the fourth shots, the last group of samples were irradiated by four shots.

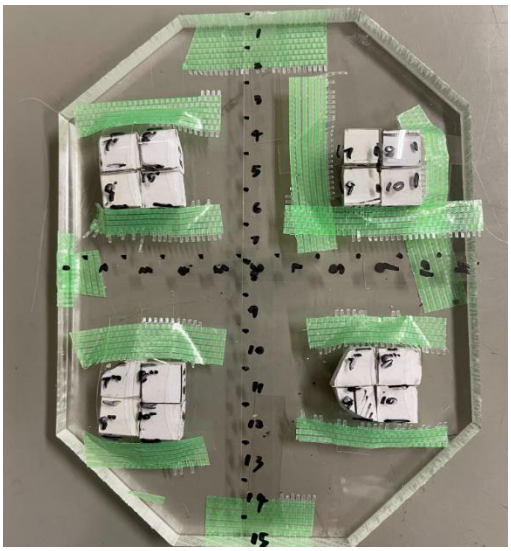

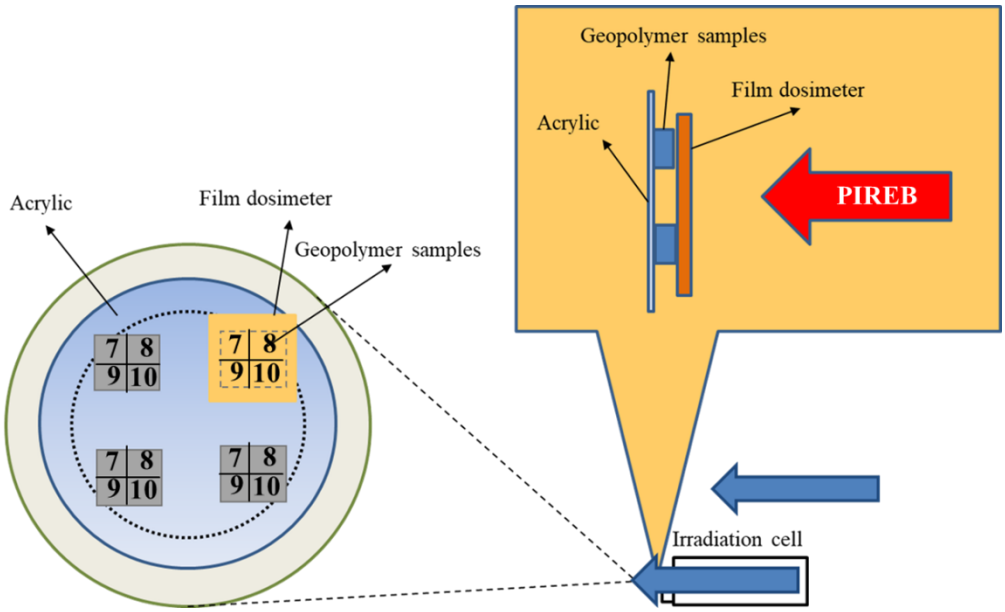


***Fig.40*** Target installation diagram in ETIGO-III

Before and after the electron radiation, the Vickers hardness was measured. The results as shown in Fig 40.

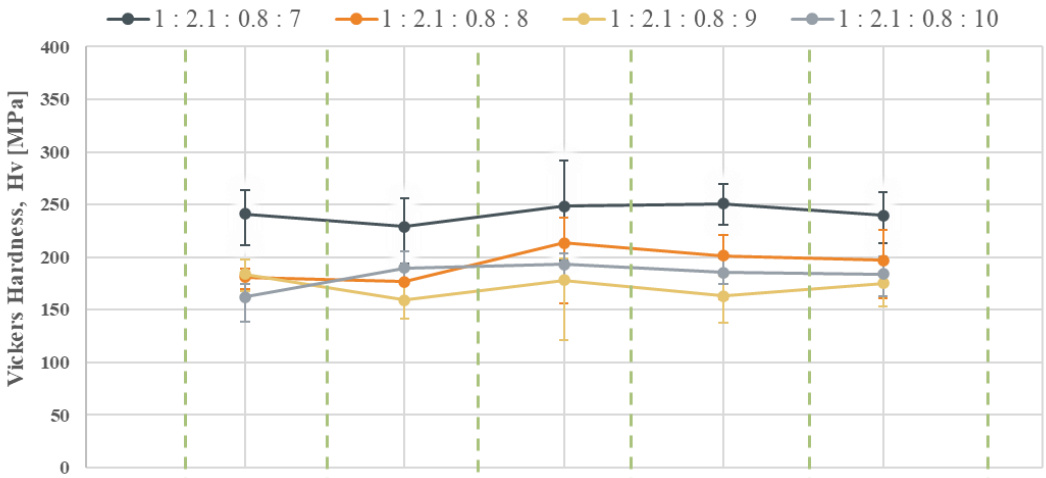


| Composition of Al: Si: K: $H_2O$ | Absorbed dose | | | | |
|---|---|---|---|---|---|
| 1: 2.1: 0.8: 7 | 0 | 7 | 9 | 9 | 14 |
| 1: 2.1: 0.8: 8 | 0 | 7 | 8 | 11 | 16 |
| 1: 2.1: 0.8: 9 | 0 | 7 | 9 | 9 | 8 |
| 1: 2.1: 0.8: 10 | 0 | 8 | 9 | 9 | 14 |

***Fig 41.*** Vickers hardness of the sample cured at room temperature for 1 day after irradiation.

When the curing temperature is the same, with the water content increasing, the Vickers hardness decreased. With the same water content (1:2.1:0.8:8,9,10), the Vickers hardness showed almost unchanged.

Due to the unchanged in Vickers unchanged up to 16 kGy. We did another electron irradiation to increase the absorbed dose. The irradiation on the table is shown in Fig. 41.

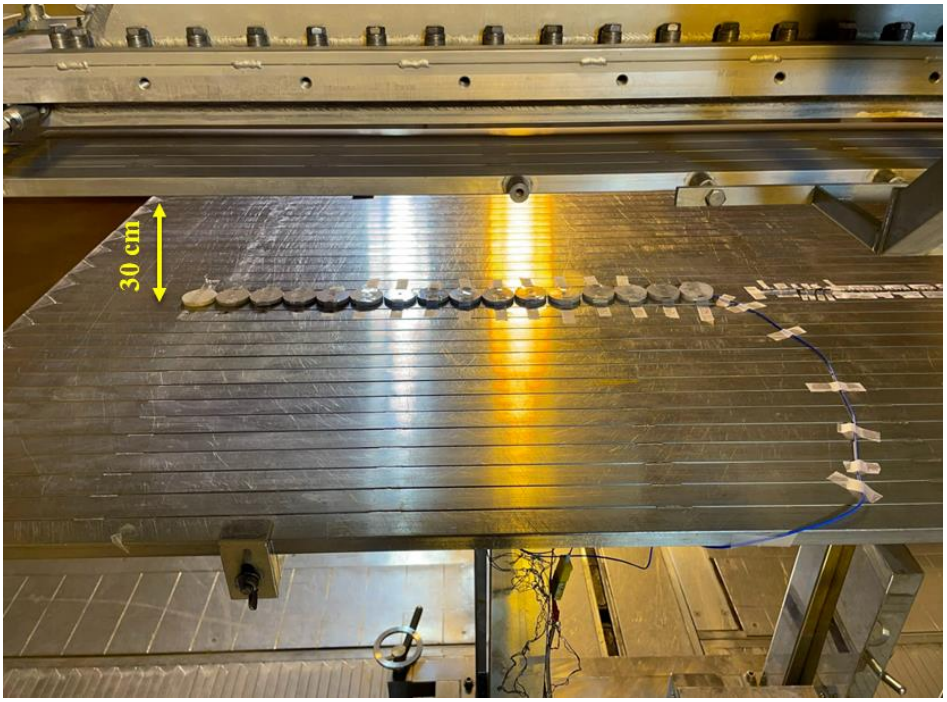


***Fig 41.*** Electron irradiation in the Cockcroft Walton accelerator.

After the electron irradiation up to 992 kGy, the Vickers hardness was shown in Figure 43 was not so much different.

Table.8. Absorption dose information

| **Dose (kGy)** | **1** | **10** | **100** | **1000** |
|---|---|---|---|---|
| **Times** | 5s | 45s | 450s | 4500s |
| **Absorption dose(kGy)** | 2 | 5 | 60 | 992 |

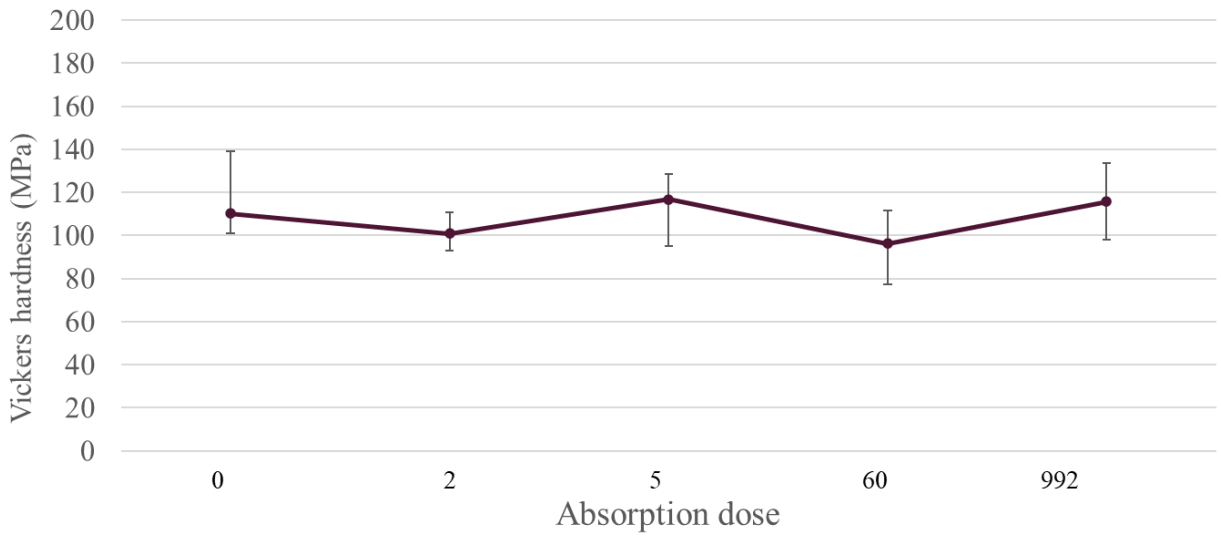


***Fig 43.*** Vickers hardness

## 6.4 Discussion

As the water content increased, the surface damage phenomenon gradually intensified. The water release can lead to intensive cracking on geopolymers. When the curing temperature was the same, with the water content increasing, the average pore size showed a slight increase and the Vickers hardness decreased. With the same water content (1:2.1:0.8:8,9,10), The average pore size and the Vickers hardness showed a decrease with the temperature increase.

In the research of Okada [71] et al. showed that a higher content of $H_2O$ to $Al_2O_3$ could lead to larger pores and larger pore volume with good water absorption properties but lower mechanical strength, while a lower content of $H_2O$ to $Al_2O_3$ resulted in denser products with smaller pore and pore volume and better water retention and mechanical strength.

After electron irradiation up to 992 kGy, the Vickers hardness was not so much different among the samples. Previous studies of silica glass materials under gamma rays have shown [72,73] the release of energy stored in the structure during the relaxation process, accompanied by a decrease in the average bridging bond Si-O-Si angle, lead to densification of the structure. There are some studies showing an increase in compressive strength of about 10% at doses up to 1 MGy [74]. The Vickers hardness did not appear to decrease with increasing electron irradiation in this experiment, which can indicate that the microstructure of the sample is still sufficiently stable under electron irradiation up to 992 kGy. This further shows that the application of potassium-based metakaolin geopolymers in the compaction of radioactive aluminum ions is possible.

## 6.5 Conclusions

Synthesis and dehydration of potassium metakaolin based geopolymer were carried out. With the same curing temperature, the average pore size showed a slight increase with the water content increase. A high-water content means that more water is released from the sample during dehydration. For the same curing time, the release of more water may cause relatively greater pressure on the pores inside the sample, thereby increasing the average pore size.

The Vickers hardness decreased with the water content increase. The high average pore size results in a relatively loose structure, which may contribute to the decrease in Vickers hardness. After electron irradiation up to 992 kGy, the Vickers hardness was not so much different for all the samples, which can indicate that the microstructure of the sample is still stable. This stability is important for the use of geopolymers for the compaction of radioactive aluminum ions.

# 7. Conclusions of this research

This thesis is aimed at research on the control of pore size distribution of potassium-based geopolymers.

The geopolymer already had a stable viscosity after one day of curing, so prolonging the initial curing time to change the subsequent container sealing conditions did not affect the porosity. And the sample was not affected by the initial curing time of geopolymer. It shows that the pores of potassium-based metakaolin geopolymer can be formed rapidly and stably.

By measuring the Vickers hardness of potassium-based metakaolin geopolymers, the geopolymers had almost no change in Vickers hardness after one day of curing compared to their fourteenth day after curing. This property provides very favorable industrial production. information, the curing time can be shortened for cost savings while still achieving high hardness levels.

Since the samples in this experiment will be used for the treatment of nuclear waste, it is particularly important to maintain the performance of the samples under radiation. In this thesis, when the sample was irradiated by electrons up to 992kGy, the Vickers hardness remained stable compared with before irradiation. These results indicate that the potassium-based geopolymer sample is possible to use in radioactive waste such as the purpose of this research to compact radioactive aluminum ions.

# 8. Suggestions

1. Exploration of the microstructure of the sample after irradiation.
    1) TG-DTA experiment after electron radiation, because the radiation usually decomposes the water in the sample, and TG-DTA can detect the period, temperature and weight loss of free water and bound water. If the water loss is confirmed before and after the experiment, we will be able to know whether free water and bound water have been lost during the radiation process.
    2) FE-SEM. To further study the influence of radiation on geopolymers, we carried out elemental analysis on the surface of the sample before and after radiation, and compared the TG-DTA result, we can further clarify the microstructure of the sample.
    3) XRD, elemental analysis will be conducted on the surface of the sample after irradiation, to know better about the microstructure.

2. Change the ratio of samples to find the ratio of samples that are more resistant to radiation.
3. Try more new raw material synthesis samples
4. Make a larger sample to better fit the actual application.

# Reference

[1] Ali Nazari; Ali Bagheri; Shadi Riahi (2011). Properties of geopolymer with seeded fly ash and rice husk bark ash. , 528(24), 7395–7401. doi:10.1016/j.msea.2011.06.027

[2] Huntzinger, Deborah N.; Gierke, John S.; Kawatra, S. Komar; Eisele, Timothy C.; Sutter, Lawrence L. (2009). Carbon Dioxide Sequestration in Cement Kiln Dust through Mineral Carbonation. Environmental Science & Technology, 43(6), 1986–1992. doi:10.1021/es802910z

[3] Kondraivendhan, B., Divsholi, B. S., & Teng, S. (2013). Estimation of Strength, Permeability and Hydraulic Diffusivity of Pozzolana Blended Concrete Through Pore Size Distribution. Journal of Advanced Concrete Technology, 11(9), 230–237. doi:10.3151/jact.11.230

[4] Davidovits J. Geopolymer Chemistry and Applications. Saint-Quentin, France: Institute Geopolymere; 2008.

[5]Dimas, D. & Giannopoulou, Ioanna & Panias, Dimitrios. (2009). Polymerization in sodium silicate solutions: A fundamental process in geopolymerization technology. Journal of Materials Science. 44. 3719-3730. 10.1007/s10853-009-3497-5.

[6] Santiago Alonso; Angel Palomo (2001). Calorimetric study of alkaline activation of calcium hydroxide–metakaolin solid mixtures. , 31(1), 25–30. doi:10.1016/s0008-8846(00)00435-x

[7] Azimi, Emy Aizat, Mohd Mustafa Al Bakri Abdullah, Liew Yun Ming, He Yong, Kamarudin Hussin and Ikmal Hakem A Aziz. “PROCESSING AND PROPERTIES OF GEOPOLYMERS AS THERMAL INSULATING MATERIALS : A REVIEW.” (2016).

[8] Ming, L.Y., Yong, H.C., Bakri, M.M.A., Hussin, K., Structure and Properties of Claybased Geopolymer Cements: A Review, Progress in Materials Science (2016), doi: http://dx.doi.org/10.1016/ j.pmatsci.2016.08.002

[9] Ikmal Hakem Aziz, Mohd Mustafa Al Bakri Abdullah, Heah Cheng Yong, Liew Yun Ming, Kamarudin Hussin, Aeslina Abdul Kadir and Emy Aizat Azimi MATEC Web Conf., 78 (2016) 01023

DOI: https://doi.org/10.1051/matecconf/20167801023

[10] Komnitsas, K. and Zaharaki, D. (2007) Geopolymerisation: A Review and Prospects for the Minerals Industry. Minerals Engineering, 20, 1261-1277.

[11] Davidovits, J. (1999) Chemistry of Geopolymeric Systems Terminology. Proceedings of Geopolymer. International Conference, France, 1999.

[12] He, Peigang; Wang, Meirong; Jia, Dechang; Yan, Shu; Yuan, Jingkun; Xu, Jiahuan; Wang, Pengfei; Zhou, Yu (2016). Effects of Si/Al ratio on the structure and properties of metakaolin based geopolymer. Ceramics International, (), S0272884216308641–. doi: 10.1016/j.ceramint.2016.06.033

[13] Hongguang Wang;Hao Wu;Zhiqiang Xing;Rui Wang;Shoushuai Dai; (2021). The Effect of Various Si/Al, Na/Al Molar Ratios and Free Water on Micromorphology and Macro-Strength of Metakaolin-Based Geopolymer . Materials, (), –. doi:10.3390/ma14143845

[14] Puertas F, Fernández-Jiménez A (2003) Mineralogical and microstructural characterization of alkali-activated fly ash/slag pastes. Cem Concr Compos 25:287–292;

[15] Puligilla S, Mondal P (2013) Role of slag in microstructural development and hardening of fly ash-slag geopolymer. Cem Concr Res 43:70–80)

[16] Faculty of Engineering, Curtin University of Technology, Perth, Australia.

[17] Bakharev, T. (2005). Geopolymeric materials prepared using Class F fly ash and elevated temperature curing. Cement and Concrete Research, 35(6), 1224-1232.

[18] Palomo, A., Grutzeck, M. W., & Blanco, M. T. (1999). Alkali-activated fly ashes: a cement for the future. Cement and Concrete Research, 29(8), 1323-1329.)

[19] (Puertas F, Fernández-Jiménez A (2003) Mineralogical and microstructural characterization of alkali-activated fly ash/slag pastes. Cem Concr Compos 25:287–292;

[20] Puligilla S, Mondal P (2013) Role of slag in microstructural development and hardening of fly ash-slag geopolymer. Cem Concr Res 43:70–80)

[21]. Albidah, Abdulrahman; Alghannam, Mohammed; Abbas, Husain; Almusallam, Tarek; Al-Salloum, Yousef (2021). Characteristics of metakaolin-based geopolymer concrete for different mix design parameters. Journal of Materials Research and Technology, 10(), 84–98. doi:10.1016/j.jmrt.2020.11.104

[22]. Albidah, A., Abadel, A., Alrshoudi, F., Altheeb, A., Abbas, H., & Al-Salloum, Y. (2020).Bond strength between concrete substrate and metakaolin geopolymer repair mortars at ambient and elevated temperatures. Journal of Materials Research and Technology, 9(5), 10732-10745.

[23] Pavel Rovnaník (2010). Effect of curing temperature on the development of hard structure of metakaolin-based geopolymer., 24(7), 1176–1183. doi:10.1016/j.conbuildmat.2009.12.023

[24] Abbass, M., Singh, G. (2022). Optimum Mix Design of Rice Husk Ash-Based Geopolymer

Concrete Based on Workability, Setting Time, and Compressive Strength Cured in Ambient Temperature Condition. In: Das, B.B., Gomez , C.P., Mohapatra, B.G. (eds) Recent Developments in Sustainable Infrastructure (ICRDSI-2020)—Structure and Construction Management. Lecture Notes in Civil Engineering, vol 221. Springer, Singapore. https://doi.org/10.1007/978- 981-16-8433-3_7

[25] Cheewaket T, Chalee W (2018) Utilization of rice husk ash-based geopolymer in hollow load-bearing concrete masonry block. J King Mongkut's Univ Technol. North Bangkok 29(2). https://doi.org/10.14416/ j.kmutnb.2018.09.005

[26] Kaur K, Singh J, Kaur M (2018) Compressive strength of rice husk ash-based geopolymer: the effect of alkaline activator. Constr Build Mater 169:188–192. https://doi.org/10.1016/j. conbuildmat.2018.02.200)

[27] Saleh, Hosam El-Din M.; Rahman, Rehab O. Abdel (2018). Cement Based Materials || Clay-Based Materials in Geopolymer Technology. , 10.5772/intechopen.71134(Chapter 14), –. doi: 10.5772/intechopen.74438

[28] Rath, B., Praveenkumar, T.R., Misgana, D. et al. Porosity of calculated clay-based geopolymer concrete incorporating natural rubber latex. Innov. Infrastructure. Solut. 7, 163 (2022). https://doi. org/10.1007/s41062-022-00769-0)

[29] Khater, H.M. Effect of silica fume on the characterization of the geopolymer materials. Int J Adv Struct Eng 5, 12 (2013). https://doi.org/10.1186/2008-6695-5-12

[30] Mohmed, Ahmed & Blash, Ahmed & Lakshmi, T.V. S. (2015). Properties of Geopolymer Concrete Produced by Silica Fume and Ground-Granulated Blast-Furnace Slag. International Journal of Science and Research (IJSR). 5. 6-391.

[31] Mangat, P. (2016). Sustainability of Construction Materials || Sustainability of alkaline-activated cementitious materials and geopolymers. , (), 459–476. doi:10.1016/B978-0-08-100370-1.00018-4.

[32] Provis, John L. (2014). Geopolymers and other alkali activated materials: why, how, and what?. Materials and Structures, 47(1-2), 11–25. doi:10.1617/s11527-013-0211-5

[33] Peiliang Cong; Yaqian Cheng; (2021). Advances in geopolymer materials: A comprehensive review . Journal of Traffic and Transportation Engineering (English Edition), –. doi:10.1016/j.jtte.2021.03.004

[34] Ghafoor, M. Talha; Khan, Qasim S.; Qazi, Asad U.; Sheikh, M. Neaz; Hadi, M.N.S. (2020).

Influence of alkaline activators on the mechanical properties of fly ash based geopolymer concrete cured at ambient temperature. Construction and Building Materials, (), 121752–. doi:10.1016/j.conbuildmat.2020.121752,

[35] Abdullah, M. M. A., H. Kamarudin, M. Bnhussain, I. Khairul Nizar, A.R. Rafiza, and Y. Zarina. "The Relationship of NaOH Molarity, Na2SiO3/NaOH Ratio, Fly Ash/Alkaline Activator Ratio, and Curing Temperature to the Strength of Fly Ash-Based Geopolymer." Advanced Materials Research 328–330 (September 2011): 1475–82. https://doi.org/10.4028/www.scientific.net/amr.328-330.1475.

[36] Mahboubi B, Guo Z, Wu H. Evaluation of durability behavior of geopolymer concrete containing Nano-silica and Nano-clay additives in acidic media. Journal of civil Engineering and Materials Application.
2019 Sep 1;3(3):163-71. [View at Google Scholar] ; [View at Publisher]

[37] Palomo A, Grutzeck MW, Blanco MT. Alkali-activated fly ashes: A cement for the future. Cement and concrete research. 1999

[38] Rocha, Thais Da Silva; Dias, Dylmar Penteado; Fraança, Fernando César Coelho; Guerra, Rafael Rangel de Salles; Marquea Rodrigues da Costa de Oliveir a (2018). Metakaolin-Based Geopolymer Mortars with Different Alkaline Activators (Na + And K + ). Construction and Building Materials, 178(), 453–461. doi:10.1016/j.conbuildmat.2018.05.172

[39] Karthiga Bakthavatchalam;Mohana Rajendran; (2021). An experimental investigation on potassium activator based geopolymer concrete incorporated with hybrid fibers . Materials Today: Proceedings, (), –. doi:10.1016/j.matpr.2021.03.506 ,

[40] Xu H, Van Deventer JS. The geopolymerisation of aluminum-silicate
minerals. International journal of mineral processing. 2000 Jun 1;59(3):247-66. [View at Google Scholar]; [View at Publisher]

[41] Phoo-ngernkham, Tanakorn; Maegawa, Akihiro; Mishima, Naoki; Hatanaka, Shigemitsu; Chindaprasirt, Prinya (2015). Effects of sodium hydroxide and sodium silicate solutions on compressive and shear bond strengths of FA–GBFS geopolymer. tion and Building Materials, 91(), 1–8. doi:10.1016/j.conbuildmat.2015.05.001

[42] Davidovits, J. (1994). Properties of geopolymer cements. Proceedings of the First International Conference on Alkaline Cements and Concretes, Kiev, Ukraine, 131-149.

[43] Vora, Prakash R.; Dave, Urmil V. (2013). Parametric Studies on Compressive Strength of

Geopolymer Concrete. Procedia Engineering, 51(), 210–219. doi:10.1016/j.proeng.2013.01.030
[44] Nguyen, Khoa Tan; Ahn, Namshik; Le, Tuan Anh; Lee, Kihak (2016). Theoretical and experimental study on mechanical properties and flexural strength of fly ash-geopolymer concrete. Construction and Building Materials, 106(), 65–77. doi:10.1016/j.conbuildmat.2015.12.033
[45] Hongling Wang; Haihong Li; Fengyuan Yan (2005). Synthesis and mechanical properties of metakaolinite-based geopolymer. , 268(1-3), 1–6. doi:10.1016/j.colsurfa.2005.01.016
[46] Tawatchai Tho-In, Vanchai Sata, Kornkanok Boonserm, Prinya Chindaprasirt, Compressive strength and microstructure analysis of geopolymer paste using waste glass powder and fly ash, Journal of Cleaner Production (2017), doi: 10.1016/j.jclepro.2017.11.125
[47] Bouaissi, Aissa; Li, Long-yuan; Al Bakri Abdullah, Mohd Mustafa; Bui, Quoc-Bao (2019). Mechanical properties and microstructure analysis of FA-GGBS-HMNS based geopolymer concrete. Construction and Building Materials, 210(), 198–209. doi:10.1016/j.conbuildmat.2019.03.202
[48] Nuruddin, M F; Malkawi, A B; Fauzi, A; Mohammed, B S; Almattarneh, H M (2016). Evolution of geopolymer binders: a review. IOP Conference Series: Materials Science and Engineering, 133(), 012052–. doi:10.1088/1757-899X/133/1/012052
[49] Ng, Connie; Alengaram, U. Johnson; Wong, Leong Sing; Mo, Kim Hung; Jumaat, Mohd Zamin; Ramesh, S. (2018). A review on microstructural study and compressive strength of geopolymer mortar, paste and concrete. Construction and Building Materials, 186(), 550–576. doi:10.1016/j.conbuildmat.2018.07.075
[50] Rees, Catherine A.; Provis, John L.; Lukey, Grant C.; van Deventer, Jannie S. J. (2007). In Situ ATR-FTIR Study of the Early Stages of Fly Ash Geopolymer Gel Formation. Langmuir, 23(17), 9076–9082. doi:10.1021/la701185g
[51] Hamidi, Rashidah Mohamed; Man, Zakaria; Azizli, Khairun Azizi (2016). Concentration of NaOH and the Effect on the Properties of Fly Ash Based Geopolymer. Procedia Engineering, 148(), 189–193. doi:10.1016/j.proeng.2016.06.568
[52] Hadi Bahmani, Davood Mostofinejad, A review of engineering properties of ultra-high-performance geopolymer concrete, Developments in the Built Environment, Volume 14, 2023,
[53] Bohra, Vinay Kumar Jain; Nerella, Ruben; Madduru, Sri Rama Chand; Rohith, P. (2020). Microstructural characterization of fly ash based geopolymer. Materials Today: Proceedings, (), S2214785320321180–. doi:10.1016/j.matpr.2020.03.338

[54] Saludung, Apriany; Ogawa, Yuko; Kawai, Kenji; Hajek, P.; Han, A.L.; Kristiawan, S.; Chan, W.T.; Ismail, M.b.; Gan, B.S.; Sriravindrarajah, R.; Hidayat, B.A. (2018). Microstructure and mechanical properties of FA/GGBS-based geopolymer. MATEC Web of Conferences, 195(), 01013–. doi:10.1051/matecconf/201819501013

[55] Farhana, Z.F.; Kamarudin, H.; Rahmat, Azmi; Al Bakri, A.M. Mustafa (2014). The Relationship between Water Absorption and Porosity for Geopolymer Paste. Materials Science Forum, 803(), 166–172. doi:10.4028/www.scientific.net/MSF.803.166

[56] Zhang, X., Bai, C., Qiao, Y., Wang, X., Jia, D., Li, H., & Colombo, P. (2021). Porous geopolymer composites: A review. Composites Part A: Applied Science and Manufacturing, 150, 106629. doi:10.1016/j.compositesa.2021.106629

[57] Yu, H, Xu, M-x, Chen, C, He, Y, Cui, Y-m. A review on the porous geopolymer preparation for structural and functional materials applications. Int J Appl Ceram Technol. 2022; 19: 1793–1813. https://doi.org/10.1111/ijac.14028

[58] https://www.tomo-e.co.jp/chemical/products/detail.php?id=25QU018

[59] http://www.sobueclay.co.jp/index.html.

[60] Kim, Jongtae, Seongho Hong, Ki-Han Park, Jin-Hyeok Kim, and Jeong-Yun Oh. 2022. "Experimental Study on Hydrogen Recombination Characteristics of a Passive Autocatalytic Recombiner during Spray Operation" Hydrogen 3, no. 2: 197-217. https://doi.org/10.3390/hydrogen3020013

[61] Lalik, E.; Kosydar, R.; Tokarz-Sobieraj, R.; Witko, M.; Szumełda, T.; Kołodziej, M.; Rojek, W.; Machej, T.; Bielańska, E.; Drelinkiewicz, A. (2015). Humidity induced deactivation of Al2O3 and SiO2 supported Pd, Pt, Pd-Pt catalysts in H2+O2 recombination reaction: The catalytic, microcalorimetric and DFT studies. Applied Catalysis A: General, 501(), 27–40. doi:10.1016/j.apcata.2015.04.029

[62] Duxson P, Provis JL, Lukey GC, Mallicoat SW, Kriven WM, van Deventer JSJ. Understanding the relationship between geopolymer composition, microstructure, and mechanical properties. Colloids Surf A: Physicochem Eng Aspects 2005; 269: 47–58.

[63] Y. Yang, T.-C. Le, I. Kudo, T.-M. Do, K. Niihara, H. Suematsu, and G. Thorogood, “Pore forming process in dehydration of metakaolin-based geopolymer,” Int. J. Ceram. Eng. Sci. (2021).

[64] John L. Provis and Jannie S. J. van Deventer “Geopolymers Structure, processing, properties and industrial applications”

[65]Davidovits,"Geopolymer, chemistry and applications", 3rd. ed., Geopolymer Institute.

[66] John L. Provis and Jannie S. J. van Deventer "Geopolymers Structure, processing, properties and industrial applications"

[67] Fernando Pacheco-Torgal, Joao Labrincha, C Leonelli, A Palomo, P Chindaprasit "Handbook of alkali-activated cements mortars and concretes"

[68] Escudier, Marcel, 'Fluids and fluid properties', Introduction to Engineering Fluid Mechanics (Oxford, 2017; online edn, Oxford Academic, 18 Jan. 2018), https://doi.org/10.1093/oso/9780198719878.003.0002

[69] T. Utsumi, T. Terasawa, I. Kudo, T. Suzuki, T. Nakayama, H Suematsu, and T. Ogawa. J. Ceram. Soc. Jpn 128 (2020) 1-5.

[70] Duxson, P., et al. (2005). "Understanding the relationship between geopolymer composition, microstructure and mechanical properties." Colloids and Surfaces A: Physicochemical and Engineering Aspects 269(1): 47-58.

[71] K. Okada, A. Ooyama, T. Isobe, Y. Kameshima, A. Nakajima, and K. J. D. MacKenzie, "Water Retention Properties of Porous Geopolymers for Use in Cooling Applications," J. Eur. Ceram. Soc., 29 [10] 1917–23 (2009).

[72] F. Piao, W.G. Oldham, E.E. Haller, J. Non-Cryst. Solids 276 (2000) 61–71.

[73] A. Sandhu, S. Singh, O. Pandey, J. Phys. D Appl. Phys. 41 (2008) 165402.

[74] Lambertin, D. et al., Influence of gamma ray irradiation on metakaolin based sodium geopolymer, J. Nucl. Mater., vol. 443, No. 1-3, 2013, pp. 311–315.